from a Kaposi's sarcoma (KS) lesion in an AIDS patient. The determination of sequences of these fragments resulted in the discovery of the KS-associated herpes virus (7). Despite the fact that RDA has been developed for detecting agents with a DNA-based genome, it can be used to detect the presence or absence of RNA in a sample by generating a cDNA intermediate (cDNA RDA) to amplify the RNA (8). Since a large quantity of ribosomal RNAs interfere with cDNA RDA, the cDNA intermediate should be synthesized from poly(A)$^+$ RNA. Therefore, it is difficult to detect RNA viruses from virus-infected cells by cDNA RDA because many viruses have no poly(A) at the end of the genome. If cDNA RDA can be applied to total RNA without interference with ribosomal RNAs, the virus genome can be amplified from total RNA of virus-infected cells by cDNA RDA.

The selection of poly(A)$^+$ RNA by using an oligo(dT) column followed by oligo(dT) priming can eliminate the influence of ribosomal RNAs on cDNA synthesis. Primers that are specific to a viral genome also efficiently eliminate the influence of ribosomal RNAs. However, prior knowledge of the virus genome is required for the construction of specific primers. In this study, based on the fact that cDNA can be primed with a mixture of oligomers, we constructed a set of oligomers that was inefficient for priming ribosomal RNAs but that normally primed most of the genome of an RNA virus (9,10). Based on the frequency distribution of hexanucleotides in ribosomal RNAs and viral sequences in current public databases, we determined a mixture of 96 hexanucleotides that rarely prime ribosomal RNAs but can prime all the known mammalian viruses listed in public databases. The results of this study show that species-independent detection of viral RNA from infected cells is possible.

MATERIALS AND METHODS

Design and synthesis of a primer mixture

A rat primary transcript, including 18S, 5.8S and 28S ribosomal RNA (V01270.1), was selected for hexanucleotide frequency analysis of ribosomal RNAs. Genomic sequences of SARS-CoV (AY291315) and bovine parainfluenza virus 3 (BPI3, NC_002161) were also selected as representatives of RNA virus (11). We created three programs, GREG, GAS and OSC (produced by C's Labs, Sapporo, Japan and licensed by Sigma–Aldrich Co. Ltd, St Louis, MO), connected to a MySQL database server (version 4.0.20). The program GREG transformed FASTA-formatted sequence to a text-formatted sequence and inserted it into a table in the MySQL database (GREG table). Using these programs, we designed a mixture of hexanucleotide primers. First, sequences were divided into hexamers, and each hexamer was classified into a pattern of hexanucleotide sequence in which $4^6 = 4096$ patterns were included. The program GAS generated frequency distributions of hexanucleotides in the sequences in the GREG table, extracted the progeny with their probabilities of hexanucleotide patterns and inserted them into a table (GAS table) of the database. We made four sets of GREG and GAS tables for rat ribosomal RNAs, a satellite repeat, BPI3 and SARS-CoV (Table 1). The program OSC listed the differences between the two GAS tables, i.e. the program selected oligomer patterns that exist in BPI3 but not in ribosomal RNAs.

Table 1. Probabilities of hexanucleotide patterns in ribosomal RNAs (V01270), a satellite-repeat (V00125), SARS coronavirus (SARS-CoV, AY291315) and bovine parainfluenza virus 3 (BPI3, NC_002161)

Pattern	Probability ($\times 10^{-3}$) Ribosomal RNA	Satellite repeat	BPI3	SARS-CoV
TCTCTC	13.54	1.28	0.25	0.11
AGAGAG	7.53	0.64	0.63	0.16
GAGAGA	7.11	1.92	0.25	0.11
CTCTCT	6.85	0.64	0.33	0.11
TCTGTC	5.67	0.00	0.28	0.25
CTTTCT	4.68	0.32	0.43	0.67
TCTTTC	4.55	0.00	0.46	0.52
TCTCTG	3.55	0.00	0.48	0.21
GTCTCT	3.43	0.64	0.28	0.21
TGTTAA	0.01	0.00	0.43	0.96
GGTCTA	0.01	0.32	0.15	0.16
ATATAT	0.00	0.00	0.96	0.13
GTGCAC	0.00	0.00	0.00	0.27
TAGTAT	0.00	0.00	0.38	0.16
GATATC	0.00	0.00	0.25	0.13
ATACTA	0.00	0.00	0.30	0.28
TATAGT	0.00	0.00	0.35	0.17
TATATA	0.00	0.00	0.81	0.05
ACTATA	0.00	0.00	0.61	0.31

The hexanucleotide patterns are aligned according to the probabilities in ribosomal RNAs. The 10 highest and lowest frequent patterns are listed in the table. A full version of the table, including all patterns, is supplemented online.

The frequency of hexamer patterns in each RNA sequence was transferred into a table of Microsoft Access. A total of 96 hexamer patterns, including those having very low frequencies or those that did not appear in ribosomal RNAs, were synthesized and mixed for use as an RT primer (Table 2, non-ribosomal hexanucleotides).

Database for mammalian viral genomic data

To estimate the frequencies of priming sites with the selected hexanucleotides, we prepared a MySQL table that included sequence data of reported viral genomes as follows. First, we downloaded all viral sequences from the FTP site of EMBL database (release date 30 June 2004) and entered them into tables (EMBL data table) of the MySQL database. The table included EMBL ID, title, annotation and sequence as fields. The annotation field included taxonomic classification of the origin of the data. We separated the words included in the annotation field into taxonomic words, such as family names, and inserted them into a new table (taxonomic table), in which EMBL IDs and taxonomic words were included. We then selected EMBL IDs of mammalian viruses with any of the viral family names listed in Table 5 from the taxonomic table. Next, sequences of mammalian viruses were divided into groups according to their species presented in the taxonomic table. To determine the targets for hexanucleotide analysis, EMBL IDs having the longest sequence in the species were selected as the estimated genomic sequence of the virus, and then, a new table named 'Sequences of viral species' was prepared. Although the longest sequence from each species was selected, some of these sequences were very short. Therefore, we eliminated sequences that were shorter than half of the common genomic size of each viral family. The resultant 1791 viral sequences were inserted into a table titled 'Genomic sequence of viral species'. The frequency of the non-ribosomal hexanucleotides was determined in sense and complementary

Table 2. Hexanucleotide patterns of non-ribosomal hexanucleotides

Motif	Motif	Motif	Motif	Motif	Motif	Motif	Motif
GATATC	GATACT	CGATAT	ACTACT	ATAGTC	CTTAGT	ACTAAG	AACTTA
TAGTAT	CGTATA	GTATAC	TAACGA	CTAGTA	CTTACA	GCATAC	ATAACG
TATAGT	GTATAG	AATCCA	CGACTA	GTACTA	TTATGC	CAATAT	ATGTTA
TATATA	CGGTTA	TAGCAC	TACTAG	TAAGTT	ATACGC	ACCGTA	TGGTAT
ATACTA	AATAGT	ATATCG	AGTAGT	ATATCC	CGCTTA	GTGCTA	TGCGTA
ATATAT	CGCATA	AATATT	GTTAAC	TCGATA	TAACGC	ACGCTA	GGATAT
GTGCAC	ATTACG	TATAGC	GTCTAC	GTACCA	GGTCAT	ATGTCG	CATAGC
ACTATA	TTAACA	CTTGTA	TACAAG	GTATCA	CTCATA	AGCTTA	CATACT
CGTAAT	AGTATC	TAGTCG	TACCAG	ATACTC	AATTTG	CGACAT	CGGATA
CTATAC	TGTTAA	GTAGAC	TGGATT	ACATTA	CTGGTA	GCTATA	TTACTA
TATACG	ACTATT	CTATAG	TCGTTA	ATATTG	TTCATG	GCTATG	ACTCGT
TATGCG	TAACCG	TAGCTA	ATAGTA	CGTCTA	GCGATA	TGTAAG	TAAGGT

strands of the sequences included in the table titled 'Genomic sequence of viral species'.

Culture of virus-infected cells and RNA extraction

The strains SARS-CoV and BPI3 were Frankfurt1 and BN-1, respectively (12–14). SARS-CoV and BPI3 were propagated by serial infection of Vero E6 and MDBK cells, respectively (15).

Vero E6 cells were routinely subcultured in 75 cm^2 flasks in DMEM (Sigma–Aldrich) supplemented with 0.2 mM/ml L-glutamine, 100 U/ml penicillin, 10 μg/ml streptomycin and 5% (v/v) fetal bovine serum (FBS) and maintained at 37°C in an atmosphere of 5% CO_2. For experimental use, the cells were split once in 25 cm^2 flasks and cultured until they reached 100% confluence. Prior to the virus infection, the culture medium was replaced with 2% FBS containing DMEM. SARS-CoV, which was isolated as Frankfurt1 and kindly provided by Dr J. Ziebuhr (16), was used in the present study. The viral infection was established in the cells with a multiplicity of infection (m.o.i) of 10. The infection of cells with SARS-CoV virus and the subsequent treatment of SARS-CoV RNA were restricted in the P4 area in the National Institute of Infectious Disease, and the work with SARS-CoV was performed in accordance with the rules for infectious pathogens that have been notified by the National Institute of Infectious Disease.

MDBK cells were maintained in Eagle's minimum essential medium (Sigma–Aldrich) supplemented with 5% FBS in a humidified atmosphere of 5% CO_2 at 37°C. The cells were infected with BPI3 at an m.o.i of 0.1. The work on infection of BPI3 was performed in accordance with the rules for pathogens that have been notified by Rakuno Gakuen University.

Extraction and *in vitro* synthesis of RNA

Total RNA was isolated using Trizol (Invitrogen, Carlsbad, CA) according to the manufacturer's instructions. Prior to cDNA synthesis, contaminated genomic DNA in the extracted RNA was digested with RNase-free DNase I (Promega, Madison, WI) at 37°C for 1 h. RNA was extracted serially with phenol and chloroform, precipitated with ethanol according to the standard protocol and subsequently used as a control RNA.

For the synthesis of a model RNA, the entire molecule of pCIneo plasmid was transcribed *in vitro* from a T7 promoter. The synthesized 5.4 kb RNA was treated with RNase-free DNase I (Promega), extracted with phenol/chloroform, precipitated with ethanol and subsequently used as a test RNA. After quantitation, the test and control RNAs were mixed to estimate the sensitivity of cDNA RDA in various conditions.

cDNA RDA

First-strand cDNA was synthesized from the mixed RNA with non-ribosomal hexanucleotides by using a double-stranded cDNA synthesis kit (Invitrogen) according to the manufacturer's protocol, i.e. the total RNA was diluted to 1 μg per μl and mixed with dNTPs, the non-ribosomal hexanucleotides, 5× reaction buffer, 0.1 M DTT and an RNase inhibitor. Reverse transcriptase (Superscript II, Invitrogen) was added, and the mixture was incubated at 50°C for 60 min. Second-strand cDNA was synthesized with *Escherichia coli* DNA polymerase (Invitrogen), *E.coli* DNA ligase (Invitrogen) and RNaseH (Invitrogen) at 16°C for 2 h. Double-stranded cDNA was digested with Dpn II, and the resultant fragments were extracted from the digest by using a silicon-membrane-based purification kit (Gene Elute Purification Kit; Sigma–Aldrich).

Linker-derived amplification of DNA fragments and selective amplification steps of cDNA RDA were performed according to the method described by Hubank and Schatz (17). Briefly, 0.1 μg of Dpn II-digested double-stranded cDNA was ligated with RBam24 and RBam12 linkers (5). An aliquot of 1 μl of the ligation solution was diluted with *Taq* mixture (10 μl of 10× *Taq* buffer, including 15 mM $MgCl_2$, and 0.2 mM each of dNTPs). The mixture was preheated to 72°C, and then, *Taq* polymerase (Promega) was added and the mixture was incubated at 72°C for 5 min to synthesize a complementary strand against the overhanging region of RBam24. This was immediately followed by a denaturation step (94°C for 2 min) and 20 cycles of PCR (94°C for 1 min and 72°C for 8 min) to non-specifically amplify 200–800 bp Dpn II-digested cDNA fragments with linkers (amplicons). After amplification, amplicons were redigested with Dpn II and purified with a silicon-membrane-based purification kit to eliminate the spliced linkers. Some amplicons, including the test RNA, were religated with JBam24 and JBam12 linkers. Amplicons with the second linkers were mixed with a large quantity of amplicons without the test RNA sequences.

The mixture was precipitated with ethanol and 3 M sodium acetate, dissolved in 4 µl of 3× EE buffer {30 mM EPPS [*N*-(2-hydroxyethyl)piperazine-*N'*-3-propanesulfonic acid], 3 mM EDTA, pH 8.0} and covered with mineral oil. After the mixture was heated to 99°C for 4 min, 1 µl of 5 M NaCl was added, and the solution was incubated at 67°C for 21 h. During this incubation period, amplicons from normal cellular RNA with a linker included in the test amplicons were hybridized with those from uninfected cells without a linker. After hybridization, the reaction mixture was diluted to 100 µl with reaction buffer of *Taq* DNA polymerase (Promega) as described above. Amplicons having the linker sequence at both ends were amplified by a denaturation step (94°C for 2 min) and 20 cycles of PCR (94°C for 1 min and 72°C for 3 min).

RNAs extracted from virus-infected cells were subjected to cDNA RDA as described above, by using amplicons synthesized from RNA obtained from uninfected cells.

Southern blot hybridization

cDNA RDA-derived fragments in quantities ranging from 100 ng to 2 µg were separated on agarose gels, blotted onto a Biodyne nylon membrane (Pall Co. Ltd, Port Washington, NY) by capillary transfer in 20× SSC (3 M sodium chloride and 0.3 M sodium citrate) for 16 h and fixed to the membrane by baking in an oven at 80°C for 30 min. pCIneo was used as a probe for the *in vitro* synthesized RNA. A random primer labelling kit (BcaBest Labeling kit, Takara Shuzo Co. Ltd, Kyoto, Japan) was used for labelling with ^{32}P and hybridized in SuperHybPlus hybridization solution (Sigma–Aldrich) according to the manufacturers' protocol.

Although amplicons are cloned into a vector to identify its sequence, according to 'Cartagena Protocol on Biosafety Text of the Protocol', amplicons from SARS-CoV-infected cells should not be cloned into any plasmid. Therefore, by performing hybridization, we identified that the sequences of amplicons derived from SARS-CoV-infected cells were identical to SARS-CoV. To determine probes for SARS-CoV, the PCR products predicted from the genomic sequence and sizes of cDNA RDA products were amplified from the SARS-CoV genome. These PCR products were purified, labelled with DIG and independently hybridized using a slit of the nylon membrane blotted with amplicons derived from SARS-CoV-infected cells. DIG labelling and hybridization were carried out according to the manufacturer's instructions provided with the DIG-hybridization kit (F. Hoffmann-La Roche Ltd, Diagnostics Division, Basel, Switzerland). Hybridization was carried out with DIG-labelled DNA probes at 65°C for 16 h in DIG-hybridization solution.

Cloning and sequence analysis

The cDNA RDA-derived fragments were respliced with Dpn II, separated on agarose gels, extracted with a silicon-membrane-based purification kit and cloned into pSPORT1 (Invitrogen). Plasmids that included cDNA RDA-derived fragments were selected by colony PCR and purified with a silicon-membrane-based purification kit. Three clones of the plasmid were sequenced along with the fragment to detect PCR errors. Sequences of the cDNA RDA-derived fragments were determined using a DYEnamic ET-terminator kit (Amersham Biosciences Corp., Piscataway, NJ) and an ABI Prism 310 sequencer (PerkinElmer Life and Analytical Sciences, Inc., Boston, MA) with M13 forward and reverse primers (Takara Shuzo). We used the BLAST program on NCBI to determine sequences that were homologous to the isolated fragments.

RESULTS

Frequency distribution of hexanucleotides within the ribosomal sequences

To predict the major RNA molecule in cellular RNA, we synthesized cDNA from RNA extracted from normal bovine cells, synthesized amplicons by using random primers, spliced them with Dpn II and finally subcloned them into pSPORT1. Among the sequences of 30 selected clones, the sequences of 25 clones and 5 clones were highly homologous to those of ribosomal RNA and a 1399 bp satellite repeat (GenBank accession no. V00125), respectively. Based on this result, ribosomal and satellite sequences were determined for analysing hexanucleotide frequency. Since the reported ribosomal sequences of mammals are highly homologous to each other, we selected rat premature 18S, 5.8S and 28S ribosomal sequences as ribosomal sequences for hexanucleotide frequency analysis. Genome sequences of SARS-CoV and BPI3 were selected as representatives of RNA viral sequence. Table 1 shows the probabilities [number of the patterns/(length of sequence × 2)] of hexanucleotides in the human ribosomal RNA, V00125 satellite repeat, BPI3 and SARS-CoV. If a random sequence is assumed, frequencies would be distributed according to the Poisson's distribution, and the average of frequency would be the same as the variance of frequency. Although the average/variance ratios of all the four sequences were <1, the ratio of ribosomal RNA was smallest in these sequences (Table 3). This value suggests that the probabilities of hexamer patterns of ribosomal RNA were strongly biased from random sequence. Based on histograms of probabilities, the distribution of the probabilities of hexamer patterns in ribosomal RNA differed greatly from those of V00125 satellite repeat or BPI3 (Figure 1). It should be noted that 8 hexanucleotides did not exist and over 90 hexanucleotides were rare in the ribosomal sequence. To determine primer sequences that do not prime ribosomal RNA but prime viral RNA, the probabilities of hexamer patterns in ribosomal RNA and satellite repeat were calculated. The hexamer patterns were then realigned in an ascending order according to the sum of probabilities, and the 1st to 96th patterns were selected as non-ribosomal hexanucleotides, i.e. we selected 96 rarest hexanucleotide patterns (Table 2, non-ribosomal hexanucleotides) in major transcripts in normal mammalian cells on the assumption that ribosomal RNA and transcripts from satellites are the most frequent transcripts in normal cells.

Table 3. Average and variances of frequencies of hexanucleotide patterns in ribosomal RNAs, a satellite repeat (V00125), bovine parainfluenza virus 3 (BPI3) and SARS coronavirus (SARS-CoV)

	Ribosomal RNAs	Satellite repeat	BPI3	SARS-CoV
Average	26.8	1.9	10.6	18.6
Variance	2156.5	2.5	96.0	188.1
Average/variance	0.012	0.76	0.11	0.099

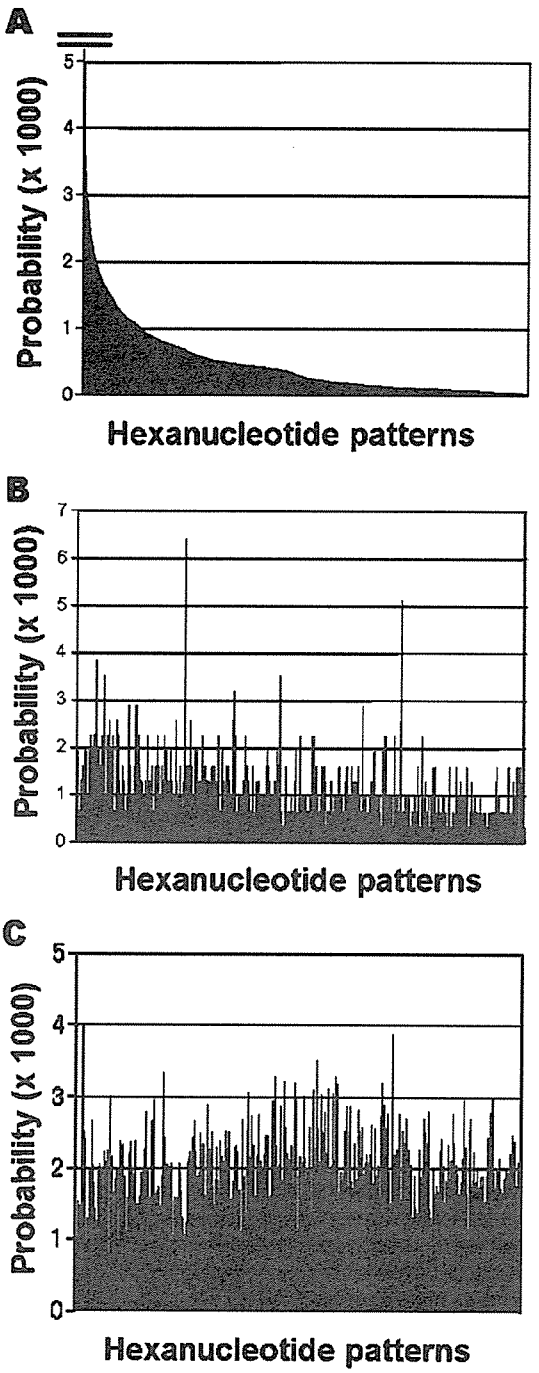

Figure 1. Histogram of probabilities of hexanucleotide patterns in ribosomal RNAs (**A**), a satellite repeat (**B**), BPI3 and SARS-CoV (**C**). From each sequence, the frequency was determined for each hexanucleotide pattern by using programs described in Materials and Methods. Probability was calculated as (frequency of a motif/total length of sequence). For simple comparison, the probabilities of ribosome RNAs and satellite repeat or SARS-CoV and BPI3 were added for each hexanucleotide pattern. Hexanucleotide patterns were aligned according to their probability in the ribosomal RNAs. When the probabilities of hexanucleotide patterns were larger than 0.005, the data were omitted.

The rarity of non-ribosomal hexanucleotides in comparison with non-V00125-satellite and random hexamers was confirmed in reported sequences of mammalian ribosomal RNAs (Table 4). The probabilities were relatively low in all the mammalian ribosomal sequences reported in GenBank. It is considered that non-ribosomal hexanucleotides inefficiently primed ribosomal RNAs in reverse transcription. On the other hand, the probabilities of non-ribosomal, non-V00125-satellite or random hexamers were different among the satellite sequences.

Frequencies of non-ribosomal hexanucleotides in viral genomic sequences

In addition to the inefficiency to prime ribosomal RNAs, efficient priming of V00125-satellite-repeat and BPI3 with non-ribosomal hexanucleotides is shown in Figure 1. To predict priming efficiency in many viruses, the probability of non-ribosomal hexanucleotides in known viral genomes was estimated. In 1791 viral sequences in 'Genomic sequences of viral species', the median probabilities of non-ribosomal hexanucleotides of all known viral sequences is $13.2–37.6 \times 10^{-3}$ (Table 5). When the average probabilities were calculated in viral families, the minimum probability was 3.7×10^{-3} in Herpesviridae and the maximum probability was 44.8×10^{-3} in Poxviridae (Table 5). These median values of probabilities in viral genomes were greater than those of ribosomal RNAs (Table 4) and comparable with those of non-V00125 and random hexamers (Table 5). These data suggest that non-ribosomal hexanucleotides prime cDNA synthesis in most viruses.

Model experiment for differentiated amplification of viral RNA by cDNA RDA

The database analysis suggests that viral RNAs were efficiently primed by non-ribosomal hexanucleotides in comparison with ribosomal RNAs. We investigated the effect of non-ribosomal hexanucleotides on cDNA synthesis by using *in vitro* synthesized plasmid RNA (artificial RNA) and total cellular RNA, including ribosomal RNAs. An autoradiogram of ^{32}P-labelled double-stranded cDNAs that were synthesized using non-ribosomal hexanucleotides or a random primer and subsequently separated by agarose gel electrophoresis is shown in Figure 2. When test and total cellular RNAs were reverse transcribed individually, the efficiencies of cDNA synthesis from artificial RNA using random and non-ribosomal hexanucleotides were almost similar; however, the efficiency of cDNA synthesis of cellular RNA was markedly lower in a non-ribosomal hexanucleotide-primed cDNA sample than in a random primer-primed cDNA sample (Figure 2A). In the mixed samples of test and total cellular RNAs, ribosomal RNAs were inefficiently reverse transcribed with non-ribosomal hexanucleotides. The total incorporated counts in non-ribosomal hexanucleotides-primed cDNAs decreased with a decrease in the proportion of the test RNA in the mixed RNA samples (Figure 2A). It is considered that the efficiency of reverse transcription depends on the proportions of the test RNA in the mixed RNAs. When approximately the same counts of cDNAs were loaded on the gel, synthesis of ribosomal RNA-derived cDNA (ribosomal cDNA) was obvious in random primer-primed cDNAs (Figure 2B).

Table 4. Total frequencies and probabilities of sense and complementary sequences of non-ribosomal, non-V00125 and random hexanucleotides in reported sequences of mammalian ribosomal RNAs and satellite repeat

Accession	Molecule	Species	Sequence length	Non-ribosomal Frequencies	Probabilities ($\times 10^{-3}$)	Non-V00125 Frequencies	Probabilities ($\times 10^{-3}$)	Random Frequencies	Probabilities ($\times 10^{-3}$)
X00686	18S rRNA	*Mus musculus*	1869	27	7.22	101	27.02	85.4	22.85
X82564	45S pre rRNA gene	*M.musculus*	22 118	281	6.35	897	20.28	974.8	22.04
M11188	18S rRNA gene. Complete	*Rattus norvegicus*	1920	27	7.03	107	27.86	87	22.66
M10098	18S rRNA gene. Complete	*Homo sapiens*	1969	27	6.86	108	27.43	89.6	22.75
U13369	Complete repeating unit	*H.sapiens*	42 999	203	2.36	1569	18.24	1743.4	20.27
M27830	28S rRNA gene. Complete	*H.sapiens*	1955	9	2.30	53	13.55	82.4	21.07
X14345	5′ external transcribed spacer of pre-ribosomal RNA	*H.sapiens*	3627	2	0.28	108	14.89	176.6	24.35
AY265350	18S rRNA gene. Complete	*S.scrofa*	2302	25	5.43	114	24.76	105.4	22.89
V01270	18S 5.8S and 28S rRNA	*R.norvegicus*	8647	71	4.11	351	20.30	405	23.42
X01117	18S rRNA sequence	*R.norvegicus*	1874	27	7.20	100	26.68	84.8	22.63
AJ311674	Partial 18S rRNA gene	*Dasypus novemcinctus*	1824	27	7.40	99	27.14	83.2	22.81
AJ311675	Partial 18S rRNA gene	*Erinaceus europaeus*	1825	27	7.40	101	27.67	82.4	22.58
AJ311673	Partial 18S rRNA gene	*Equus caballus*	1824	25	6.85	100	27.41	82.8	22.70
X06778	18S rRNA	*Oryctolagus cuniculus*	1863	30	8.05	103	27.64	84.6	22.71
AJ311678	Partial 18S rRNA gene	*Vombatus ursinus*	1845	28	7.59	101	27.37	81.8	22.17
AJ311676	Partial 18S rRNA gene	*Monodelphis domestica*	1847	28	7.58	100	27.07	81.6	22.09
AJ311677	Partial 18S rRNA gene	*Didelphis virginiana*	1847	28	7.58	100	27.07	81.6	22.09
AJ311679	Partial 18S rRNA gene	*Ornithorhynchus anatinus*	1850	28	7.57	102	27.57	82.8	22.38
V00125	Repeated unit of bovine 1.715 satellite DNA	*Bos taurus*	1399	0	0.00	0	0.00	66.6	23.80
J00036	Thymus satellite I	*B.taurus*	1402	3	1.07	5	1.78	64.2	22.90
U59381	Tetranucleotide microsatellite repeat	*H.sapiens*	1032	2	0.97	29	14.05	35	16.96
AY153482	Microsatellite PDE6B sequence	*S.scrofa*	1895	20	5.28	64	16.89	82.6	21.79
AF298194	Clone pW-1 microsatellite III	*H.sapiens*	1524	17	5.58	31	10.17	71	23.29
AY339973	Clone 1 satellite sequence	*Canis familiaris*	1200	17	7.08	41	17.08	52.6	21.92
U53349	Chromosome 10 microsatellite	*R.norvegicus*	1070	21	9.81	32	14.95	36.2	16.92
AJ295050	Alpha satellite 5CEN-P7	*H.sapiens*	1382	31	11.22	61	22.07	58.8	21.27
AB023433	Satellite sequence	*R.norvegicus*	2845	86	15.11	136	23.90	125	21.97
AY145450	Microsatellites D6Wum35 and D6Wum34	*M.musculus*	1704	71	20.83	103	30.22	73.4	21.54
AF181667	Polymorphic microsatellite sequence	*H.sapiens*	3650	201	27.53	213	29.18	164.4	22.52
AF259760	Microsatellite MNS-87 and MNS-88	*Ovis aries*	1074	86	40.04	38	17.69	48.2	22.44
U10629	Chromosome 4 satellite	*H.sapiens*	1060	116	54.72	48	22.64	55.4	26.13

Sequences of the non-V00125 and random hexamers are supplemented online. Probabilities of the hexanucleotide-sets in 2464 reported satellite repeat are also supplemented online.

Table 5. Number of species and maximum, minimum and median probabilities [median (minimum – maximum)] ($\times 10^{-3}$) of non-ribosomal, non-V00125-satellite-repeat and random hexamers hexanucleotides in known viral species

Family	Number of species	Non-ribosomal	Non-V00125	Random hexamers
Adenoviridae	25	15.3 (6.5–28.3)	25.0 (19.4–47.1)	23.8 (22.8–47.6)
Arenaviridae	8	17.0 (13.1–19.2)	26.0 (23.3–27.6)	24.5 (23.8–25.1)
Astroviridae	7	17.4 (14.5–19.2)	23.9 (22.4–25.6)	24.3 (23.5–25.2)
Bornaviridae	1	20.0 (20.0–20.0)	21.8 (21.8–21.8)	23.7 (23.7–23.7)
Bunyaviridae	26	22.8 (11.8–30.7)	26.2 (21.8–29.7)	23.7 (23.1–25.3)
Caliciviridae	23	13.2 (7.1–19.3)	23.5 (19.1–26.5)	24.1 (23.4–25.4)
Coronaviridae	51	24.2 (23.9–31.4)	25.3 (25.2–29.9)	23.6 (23.5–24.3)
Filoviridae	3	21.9 (20.8–22.6)	24.9 (24.4–26.2)	25.0 (24.5–25.1)
Flaviviridae	53	14.1 (8.6–23.4)	22.4 (19.0–25.9)	24.0 (21.6–25.2)
Hepadnaviridae	14	16.6 (9.7–27.2)	21.6 (18.0–25.3)	24.0 (21.3–24.5)
Herpesviridae	31	15.0 (3.7–29.2)	22.6 (16.4–27.2)	23.5 (22.8–24.5)
Iridoviridae	3	17.7 (14.1–25.2)	23.3 (20.8–29.3)	23.5 (21.9–23.6)
Orthomyxoviridae	1029	17.6 (6.3–29.7)	24.3 (16.2–32.9)	24.3 (20.0–27.9)
Papillomaviridae	123	24.7 (7.7–34.3)	24.9 (18.7–28.9)	23.2 (21.1–25.0)
Parvoviridae	59	20.5 (6.3–35.9)	25.0 (19.5–31.2)	23.8 (21.6–25.1)
Picornaviridae	90	19.3 (7.1–30.6)	24.3 (19.0–29.0)	24.0 (22.6–25.1)
Polyomaviridae	16	18.4 (14.0–28.5)	22.0 (20.6–26.4)	23.6 (22.3–24.7)
Poxviridae	21	37.6 (8.2–44.8)	26.9 (22.7–32.0)	22.9 (21.3–24.0)
Reoviridae	89	28.4 (12.9–38.4)	26.2 (19.2–31.5)	23.8 (20.7–25.8)
Retroviridae	86	17.0 (9.9–27.6)	22.1 (18.2–26.8)	23.3 (21.6–24.6)
Rhabdoviridae	14	16.8 (9.2–25.3)	22.7 (19.0–26.3)	23.6 (23.1–24.2)
Togaviridae	19	20.0 (7.6–24.3)	23.3 (20.1–25.1)	23.7 (22.7–24.5)

Sequences for species were selected according to their length as described in Materials and Methods. The total probability in each species was calculated as the summation of probabilities of all non-ribosomal hexanucleotides in sense and complementary sequences of a viral genomic sequence that was selected as described in Materials and Methods. The probabilities of non-ribosomal hexanucleotides in 1791 virus genomic sequences are supplemented online.

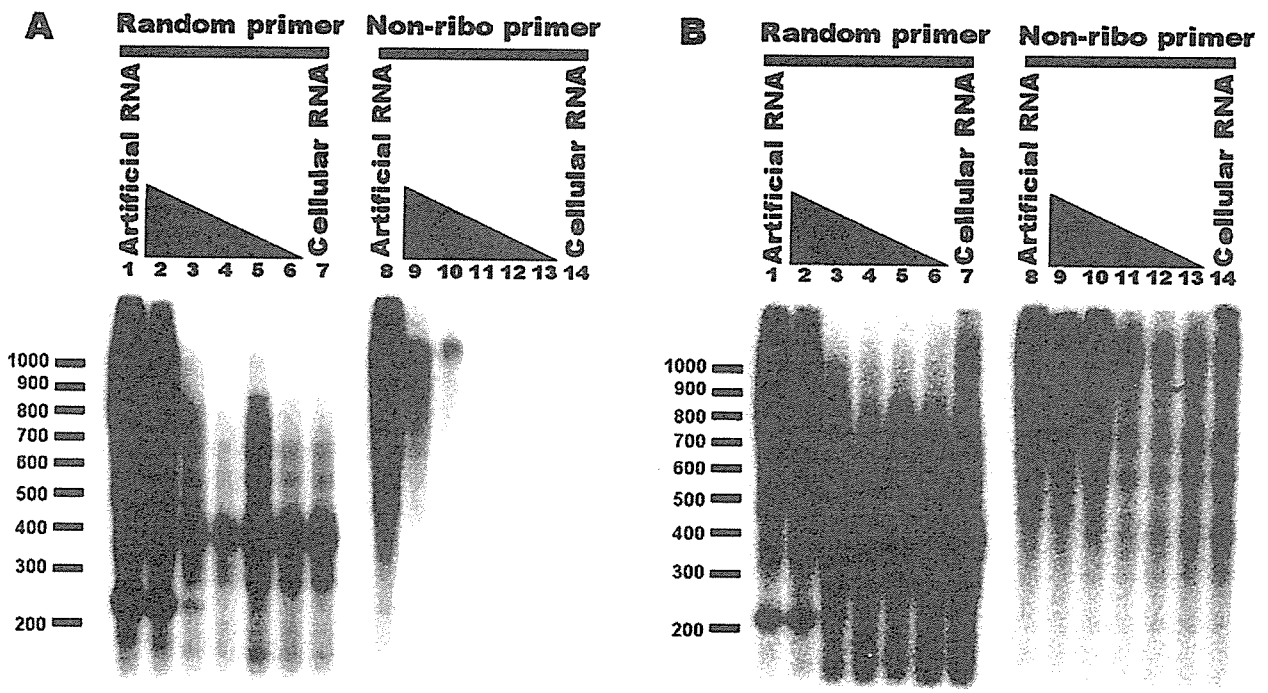

Figure 2. Autoradiogram of ^{32}P-labelled double-stranded cDNA synthesized from mixtures consisting of artificial RNA and total cellular RNA. *In vitro* transcribed RNA was synthesized from pCIneo plasmid and mixed with total cellular RNA extracted from rat2 cells in weight proportions 1:0 (lanes 1 and 8), 1:1 (lanes 2 and 9), 1:10 (lanes 3 and 10), 1:100 (lanes 4 and 11), 1:300 (lanes 5 and 12), 1:1000 (lanes 6 and 13) and 0:1 (lanes 7 and 14). One microgram of mixed RNA was reverse transcribed using random (lanes 1–7) or non-ribosomal (lanes 8–14) hexanucleotides and a second-strand cDNA was then synthesized with RNaseH, DNA polymerase and DNA ligase according to the method described in Materials and Methods. One-tenth of the volume of synthesized cDNAs was loaded on agarose gel (**A**). Loaded volumes were corrected to include the same amounts of ^{32}P in each sample (**B**). Positions and sizes (bp) of markers are present on the left.

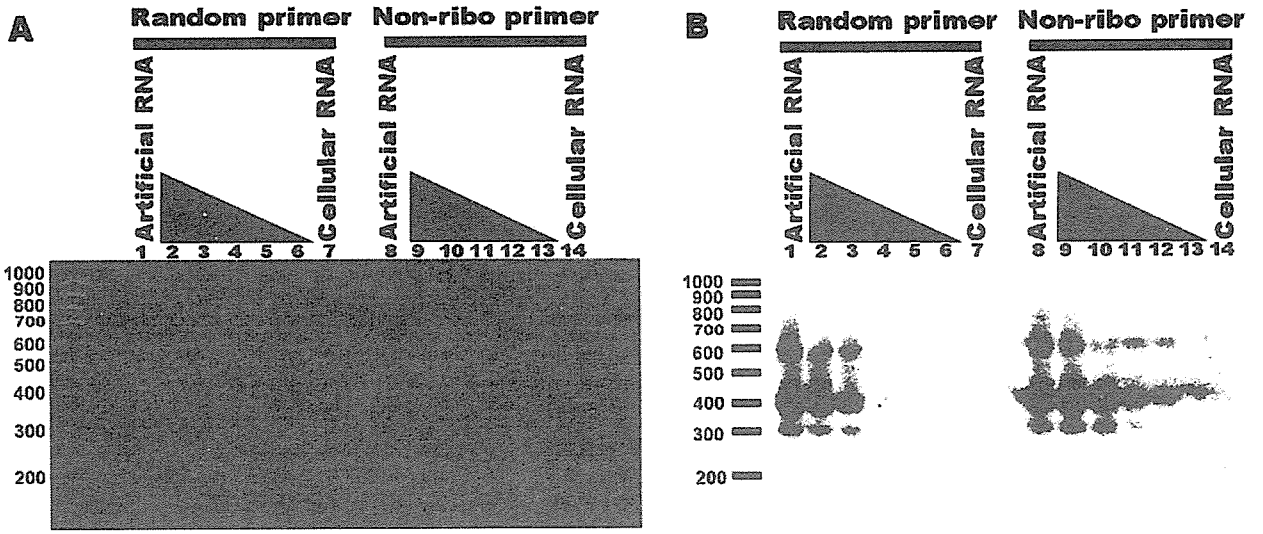

Figure 3. Agarose gel electrophoresis of RDA products (**A**) and its hybridized autoradiogram (**B**). *In vitro* transcribed RNA and total cellular RNA were mixed as described in the legend to Figure 2. Double-stranded cDNAs were synthesized and subjected to RDA as described in Materials and Methods. One-twentieth of the volume of the amplified products was separated on 3% agarose gel and stained with ethidium bromide (**A**), blotted onto a nylon membrane and hybridized with ^{32}P-labelled pCIneo (**B**). Positions and sizes (bp) of markers are present on the left.

On the other hand, the synthesis of ribosomal cDNA was not obvious in the cDNA primed with non-ribosomal hexanucleotides. A relatively large cDNA derived from artificial RNA could be observed even when a smaller proportion of test RNA was mixed with cellular RNA and non-ribosomal hexanucleotide-primed samples. These data suggest that the relative amount of test RNA-derived cDNA is greater in non-ribosomal hexanucleotides-primed samples than in random primer-primed samples.

After the first round of cDNA RDA, amplified fragments were observed on agarose by staining with ethidium bromide. The bands that corresponded to artificial RNA could be observed in 1:0, 1:1 and 1:10 (test:total cellular RNAs) mixtures when cDNAs were primed with a random primer. On the other hand, these bands could be observed in 1:0 to 1:300 RNA mixtures when cDNA was primed with non-ribosomal hexanucleotides (Figure 3A). This amplification of test RNA was confirmed by hybridization with pCIneo, which was a template for *in vitro* RNA synthesis (Figure 3B). The hybridized bands were observed even in a lane corresponding to 1:1000 RNA mixture. When cDNA was primed with a random primer, the hybridized bands could not be observed in 1:100, 1:300 and 1:1000 RNA mixtures. These data suggest that the lower limit of the test RNA amplification decreased at least 30 times when non-ribosomal hexanucleotides were used for reverse transcription when compared with the data obtained by using a random primer.

Detection of BPI3 and SARS-CoV sequences from infected cell RNA

To amplify virus sequence from infected cells, we subtracted amplicons derived from uninfected cells from those derived from virus-infected cells. Amplicons with linkers derived from the infected cells were mixed with amplicons without linkers

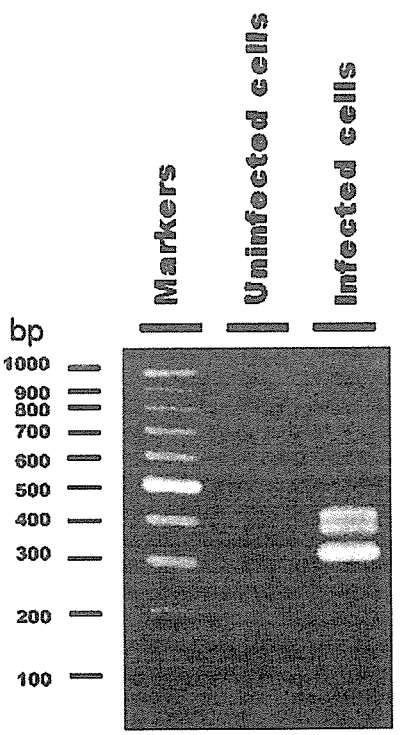

Figure 4. Agarose gel electrophoresis of RDA products from RNA extracted from bovine parainfluenza virus 3-infected cells. Double-stranded cDNA was synthesized from RNA of bovine parainfluenza virus 3-infected MDBK cells and subjected to RDA. Mock-infected cells were used for the synthesis of driver amplicons for RDA. One-twentieth of the volume of the amplified products was separated on 3% agarose gel and stained with ethidium bromide. RDA product from the uninfected control cells was used as a negative control.

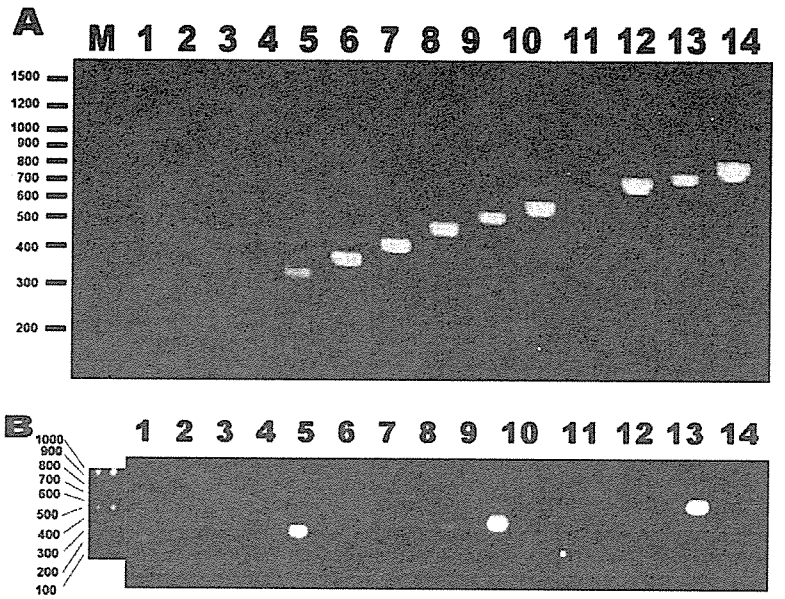

Figure 5. Agarose gel electrophoresis of RDA products with PCR products used for probes for hybridization (**A**) and a hybridized fluorogram (**B**). RNA was extracted from SARS-CoV-infected cells and subjected to RDA according to the method described in Materials and Methods. Mock-infected cells were used for the synthesis of driver amplicons for RDA. One-twentieth of the volume of the amplified products was separated on 3% agarose gels and blotted on a Nylon membrane. The membrane was then cut into slits that contained the lane showing the presence of DNA. On the other hand, the PCR fragments predicted to be amplified in the RDA reaction were amplified and subsequently ascertained by agarose gel electrophoresis (A). The amplified genomic fragments of SARS-CoV were Dig-labelled and used as probes for hybridization to each slit of the Nylon membrane containing the RDA product. Hybridization was performed in separate hybridization bags. After washing with 1× SSC and 0.1% SDS solution, the hybridized probes were detected on a fluorogram (B). Positions and sizes (bp) of markers are present on the left.

derived from uninfected cells at the ratio of 1:100 before a hybridization step of cDNA RDA. At the end of the first round of cDNA RDA, the ladders of amplified fragments were generated from BPI3-infected cells when non-ribosomal hexanucleotides were used (Figure 4). No cDNA RDA-derived bands were obvious when a random primer was used for reverse transcription (data not shown). Amplified fragments from cDNA RDA of BPI3-infected cells were cloned into pSPORT1 plasmid, and the sequences were determined. The sequences of all the cloned fragments from cDNA RDA were identical to the sequence of the BPI3 genome. These data suggest that cDNA RDA with non-ribosomal hexanucleotides enables the identification of the BPI3 genome sequence from infected cells.

Similar to BPI3, cDNA fragments derived from SARS-CoV were also amplified from SARS-CoV-infected cells (Figure 5). Viral origin of the amplified fragments was confirmed by hybridization (Figure 5B) and PCR amplification by SARS-CoV-specific primers (Figure 5A). These results indicate that genomic fragments of SARS-CoV can also be isolated by this method.

DISCUSSION

Reduction of influence of ribosomal RNA on cDNA synthesis by non-ribosomal hexanucleotides

It is well known that 3–5% and 30% of cellular RNA are estimated to be messenger and ribosomal RNA, respectively. The frequency of ribosomal RNA has been estimated by competitive PCR and real-time PCR to be 10 000 copies per cell (18). The amount of ribosomal RNA has been reported to be 1000-fold greater than that of frequently transcribed mRNA, such as beta actin and G6PDH. Thus, the repertoire of cDNA would be strongly affected by ribosomal RNA. This influence of ribosomal RNA has been avoided by oligo(dT) selection. Alternative strategy for the elimination of ribosomal RNA from total RNA, however, has not been developed. Therefore, there have been only a few applications of cDNA RDA for non-poly(A) RNA, such as those in viral genomes. In this study, we developed a new strategy for the elimination of ribosomal RNA in cDNA RDA through the construction of a hexanucleotide mixture and demonstrated its efficiency in cDNA RDA.

The main purpose of PCR is specific amplification of a gene. However, methods using multiple primers for simultaneous gene amplification have been recently employed for DNA chip methods. In order to simultaneously detect multiple genes by using a DNA chip, mixed oligonucleotides have been used as a primer for reverse transcription. This usage of mixed primers was based on the assumption that the specificity of primers was equal to the summation of the specificity of each primer. Thus, we searched for primers that do not prime ribosomal RNAs by frequency analysis of hexanucleotides. The frequency and distribution of oligonucleotides in mammalian and viral genomes have been studied to search for common motifs that might be used for controlling cellular functions (19–23). Volinia *et al.* (22) found sets of common decamers that can be used for the control of transcription control signals or for the common amplification of viruses. Programs for frequency

analysis have been useful for searching common oligonucleotides in many subsets of sequences. On the other hand, database programming is useful not only for searching common oligonucleotides but also for searching oligonucleotides that do not exist in a subset of sequences. In this study, we found that there were hexanucleotide patterns that were rare or that did not exist in ribosomal RNA sequences. We also showed that sequences of 96 selected non-ribosomal hexanucleotides are normally present in known viral sequences (Table 5).

Improvement of detection efficiency of extracellular RNA on cDNA RDA

In the experiment for the determination of the effect of non-ribosomal hexanucleotides, we used a mixture of artificially synthesized and total cellular RNAs. The probabilities of hexanucleotide patterns in the sequence of pCIneo was different from ribosomal RNA (18.4×10^{-3}, 22.4×10^{-3} and 23.0×10^{-3} for non-ribosomal, non-V00125 and random hexamers, respectively). The artificially synthesized RNA included 30 priming sites for non-ribosomal hexanucleotides and was efficiently reverse transcribed (Figure 2). In the model experiments, cDNA RDA with non-ribosomal hexanucleotides efficiently reverse transcribed and specifically amplified the extracellular test RNA in the mixed RNA (Figure 3). cDNA RDA-derived detection of the artificial RNA was 30-fold more sensitive when non-ribosomal hexanucleotides were used than when random hexamers were used. These results suggest that non-ribosomal hexanucleotides dramatically improve the detection efficiency of cDNA RDA.

Application of non-ribosomal hexanucleotides for viral detection

The common existence of non-ribosomal hexanucleotides in known viral genomes (Table 5) and the improved sensitivity for the amplification of a non-ribosomal sequence in the mixed RNAs (Figure 3) suggest that non-ribosomal hexanucleotides could be used for non-specific detection of a viral sequence in infected cells. However, the sensitivity for sequence detection may be low when compared with that of common PCR using specific primers. Thus, the usage of this method might be restricted to infected cells that contain many copies of a virus.

The copy number of RNA viruses is dependent on the virus species, host cells and replicative and productive state of viruses. In our experiment, we detected 3 ng of contaminated RNAs in 1 μg of total RNA. Although this sensitivity is considerably lower than that of normal PCR, our experiments on SARS-CoV and BPI3 suggest that the sensitivity of cDNA RDA with non-ribosomal hexanucleotides is sufficient to detect these viruses in productively infected cells. Additionally, this method can be applied to most productive viruses, since sense and complementary sequences of non-ribosomal hexanucleotides were found to exist in most of the known virus sequences in GenBank (Table 5). In conclusion, this method could be applied as an alternative method for the detection of any emerging viruses.

SUPPLEMENTARY MATERIAL

Supplementary Material is available at NAR Online.

ACKNOWLEDGEMENTS

This work was funded by a grant from the Ministry of Economy, Trade and Industry of Japan (to D.E.) and by a grant from the Ministry of Environment of Japan. Funding to pay the Open Access publication charges for this article was provided by New Industry Creative Type Technology R&D Promotion Program in the Hokkaido Bureau of Economy, Trade and Industry.

Conflict of interest statement. None declared.

REFERENCES

1. Rota,P.A., Oberste,M.S., Monroe,S.S., Nix,W.A., Campagnoli,R., Icenogle,J.P., Penaranda,S., Bankamp,B., Maher,K., Chen,M.H. *et al.* (2003) Characterization of a novel coronavirus associated with severe acute respiratory syndrome. *Science*, **300**, 1394–1399.
2. Gao,S.J. and Moore,P.S. (1996) Molecular approaches to the identification of unculturable infectious agents. *Emerg. Infect. Dis.*, **2**, 159–167.
3. Holmes,E.C. and Rambaut,A. (2004) Viral evolution and the emergence of SARS coronavirus. *Philos. Trans. R. Soc. Lond., B, Biol. Sci.*, **359**, 1059–1065.
4. Pavlovic-Lazetic,G.M., Mitic,N.S. and Beljanski,M.V. (2004) Bioinformatics analysis of SARS coronavirus genome polymorphism. *BMC Bioinformatics*, **5**, 65.
5. Lisitsyn,N., Lisitsyn,N. and Wigler,M. (1993) Cloning the differences between two complex genomes. *Science*, **259**, 946–951.
6. Chang,Y., Cesarman,E., Pessin,M.S., Lee,F., Culpepper,J., Knowles,D.M. and Moore,P.S. (1994) Identification of herpesvirus-like DNA sequences in AIDS-associated Kaposi's sarcoma. *Science*, **266**, 1865–1869.
7. Staskus,K.A., Zhong,W., Gebhard,K., Herndier,B., Wang,H., Renne,R., Beneke,J., Pudney,J., Anderson,D.J., Ganem,D. *et al.* (1997) Kaposi's sarcoma-associated herpesvirus gene expression in endothelial (spindle) tumor cells. *J. Virol.*, **71**, 715–719.
8. Hubank,M. and Schatz,D.G. (1994) Identifying differences in mRNA expression by representational difference analysis of cDNA. *Nucleic Acids Res.*, **22**, 5640–5648.
9. Tian,H., Cao,L., Tan,Y., Williams,S., Chen,L., Matray,T., Chenna,A., Moore,S., Hernandez,V., Xiao,V. *et al.* (2004) Multiplex mRNA assay using electrophoretic tags for high-throughput gene expression analysis. *Nucleic Acids Res.*, **32**, e126.
10. Eldering,E., Spek,C.A., Aberson,H.L., Grummels,A., Derks,I.A., de Vos,A.F., McElgunn,C.J. and Schouten,J.P. (2003) Expression profiling via novel multiplex assay allows rapid assessment of gene regulation in defined signalling pathways. *Nucleic Acids Res.*, **31**, e153.
11. Bailly,J.E., McAuliffe,J.M., Skiadopoulos,M.H., Collins,P.L. and Murphy,B.R. (2000) Sequence determination and molecular analysis of two strains of bovine parainfluenza virus type 3 that are attenuated for primates. *Virus Genes*, **20**, 173–182.
12. Iwai,H., Morioka,A., Shoya,Y., Obata,Y., Goto,M., Kirisawa,R., Okada,H. and Yoshino,T. (1998) Protective effect of passive immunization against TNF-alpha in mice infected with Sendai virus. *Exp. Anim.*, **47**, 49–54.
13. Mizutani,T., Fukushi,S., Saijo,M., Kurane,I. and Morikawa,S. (2004) Importance of Akt signaling pathway for apoptosis in SARS-CoV-infected Vero E6 cells. *Virology*, **327**, 169–174.
14. Mizutani,T., Fukushi,S., Saijo,M., Kurane,I. and Morikawa,S. (2004) Phosphorylation of p38 MAPK and its downstream targets in SARS coronavirus-infected cells. *Biochem. Biophys. Res. Commun.*, **319**, 1228–1234.
15. Mizutani,T., Fukushi,S., Murakami,M., Hirano,T., Saijo,M., Kurane,I. and Morikawa,S. (2004) Tyrosine dephosphorylation of STAT3 in SARS coronavirus-infected Vero E6 cells. *FEBS Lett.*, **577**, 187–192.
16. Thiel,V., Ivanov,K.A., Putics,A., Hertzig,T., Schelle,B., Bayer,S., Weissbrich,B., Snijder,E.J., Rabenau,H., Doerr,H.W. *et al.* (2003) Mechanisms and enzymes involved in SARS coronavirus genome expression. *J. Gen. Virol.*, **84**, 2305–2315.
17. Hubank,M. and Schatz,D.G. (1994) Identifying differences in mRNA expression by representational difference analysis of cDNA. *Nucleic Acids Res.*, **22**, 5640–5648.

18. Monk,R.J., Meyuhas,O. and Perry,R.P. (1981) Mammals have multiple genes for individual ribosomal proteins. *Cell*, **24**, 301–306.
19. Gambari,R., Volinia,S., Nesti,C., Scapoli,C. and Barrai,I. (1994) A set of Alu-free frequent decamers from mammalian genomes enriched in transcription factor signals. *Comput. Appl. Biosci.*, **10**, 501–508.
20. Scapoli,C., Rodriguez-Larralde,A., Volinia,S. and Barrai,I. (1993) Enrichment of oligonucleotide sets with transcription control signals. III: DNA from non-mammalian vertebrates. *Comput. Appl. Biosci.*, **9**, 647–651.
21. Scapoli,C., Rodriguez-Larralde,A., Volinia,S., Beretta,M. and Barrai,I. (1994) Identification of a set of frequent decanucleotides in plants and in animals. *Comput. Appl. Biosci.*, **10**, 465–470.
22. Volinia,S., Scapoli,C., Gambari,R., Barale,R. and Barrai,I. (1991) A set of viral DNA decamers enriched in transcription control signals. *Nucleic Acids Res.*, **19**, 3733–3740.
23. Volinia,S., Scapoli,C., Gambari,R., Barale,R. and Barrai,I. (1992) Enrichment of oligonucleotide sets with transcription control signals. II: Mammalian DNA. *Nucleic Acids Res.*, **20**, 551–556.

Available online at www.sciencedirect.com
SCIENCE DIRECT®
Journal of Virological Methods 125 (2005) 181–186
Journal of Virological Methods
www.elsevier.com/locate/jviromet

Recombinant nucleocapsid protein-based IgG enzyme-linked immunosorbent assay for the serological diagnosis of SARS

Masayuki Saijo[a,*], Toshio Ogino[b], Fumihiro Taguchi[b], Shuetsu Fukushi[a], Tetsuya Mizutani[a], Tsugunori Notomi[c], Hidetoshi Kanda[c], Harumi Minekawa[c], Shutoku Matsuyama[b], Hoang Thuy Long[d], Nguyen Thi Hong Hanh[d], Ichiro Kurane[a], Masato Tashiro[b], Shigeru Morikawa[a]

[a] *Special Pathogens Laboratory, Department of Virology 1, National Institute of Infectious Diseases, 4-7-1 Gakuen, Musashimurayama 208-0011, Tokyo, Japan*
[b] *Laboratory of Respiratory Viral Diseases and SARS, Department of Virology 3, National Institute of Infectious Diseases, 4-7-1 Gakuen, Musashimurayama 208-0011, Tokyo, Japan*
[c] *Biochemical Research Laboratory, Eiken Chemical Co., Ltd., 1381-3 Shimoishigami, Ohtawara, Tochigi 324-0036, Japan*
[d] *National Institute of Hygiene and Epidemiology, 1, Yersin Street, Hanoi, Vietnam*

Received 6 October 2004; received in revised form 19 January 2005; accepted 26 January 2005
Available online 24 February 2005

Abstract

The recombinant nucleocapsid protein (rNP) of severe acute respiratory syndrome (SARS) coronavirus (SARS-CoV) was expressed in a baculovirus system. The purified SARS-CoV rNP was used as an antigen for detection of SARS-CoV antibodies in IgG enzyme-linked immunosorbent assay (ELISA). The ELISA was evaluated in comparison with neutralizing antibody assay and the authentic SARS-CoV antigen-based IgG ELISA. Two-hundred and seventy-six serum samples were collected from health care workers in a hospital in which a nosocomial SARS outbreak took place and used for evaluation. The SARS-CoV rNP-based IgG ELISA has 92% of sensitivity and specificity compared with the neutralizing antibody assay and 94% sensitivity and specificity compared with the authentic SARS-CoV antigen-based IgG ELISA. The results suggest that the newly developed SARS-CoV rNP-based IgG ELISA is a valuable tool for the diagnosis and seroepidemiological study of SARS. The SARS-CoV rNP-based IgG ELISA has an advantage over the conventional IgG ELISA in that the antigen can be prepared by laboratory workers without the risk of infection.

Keywords: Recombinant nucleocapsid protein; SARS; IgG ELISA; Neutralizing antibody assay

1. Introduction

Severe acute respiratory syndrome (SARS), an emerging virus infection of the respiratory organs with a high mortality rate in humans, was first reported in Guangdong province, in southern part of China, in November 2002 and spread to Hong Kong, Vietnam, Singapore and other countries worldwide through human-to-human transmission (CDC, 2003; Lee et al., 2003; Poutanen et al., 2003; Tsang et al., 2003). Approximately 8000 patients were reported and about 800 died in the last SARS outbreak from November 2002 to July 2003 (WHO).

The causative agent, SARS coronavirus (SARS-CoV), was isolated from patients with SARS and was identified as a novel coronavirus. SARS-CoV was transmitted from human to human, and the mortality rate is high. SARS-CoV is regarded as a viral pathogen that must be handled in high containment laboratories with a biosafety level (BSL)-3 and BSL-4.

If a recombinant protein of SARS-CoV can be used as an antigen for serological diagnosis of SARS-CoV infections,

* Corresponding author. Tel.: +81 42 561 0771; fax: +81 42 561 2039.
E-mail address: msaijo@nih.go.jp (M. Saijo).

0166-0934/$ – see front matter © 2005 Elsevier B.V. All rights reserved.
doi:10.1016/j.jviromet.2005.01.028

it offers an advantage in the preparation of a SARS-CoV antigen because the recombinant protein of SARS-CoV can be produced without a risk of SARS-CoV-infections among laboratory workers. In the present study, we developed an IgG enzyme-linked immunosorbent assay (ELISA) in which a recombinant nucleocapsid protein (rNP) of SARS-CoV (SARS-CoV rNP) was used as an antigen, and evaluated the efficacy of the ELISA using serum samples collected from the health care workers in a hospital that was hit by a SARS-nosocomial outbreak.

2. Materials and methods

2.1. Virus

The SARS-CoV (HKU39849) used in this study was kindly supplied by Prof. J.S. Malik Peiris, Department of Microbiology, University of Hong Kong, Hong Kong Special Administrative Region.

2.2. Cells

Vero E6 cells purchased from the American Type Cell Collection (Manassas, VA) were grown in Eagle's minimum essential medium (MEM) supplemented with penicillin G and streptomycin and with 5% fetal bovine serum. The FBS was confirmed to have no inhibitory effect on the growth of SARS-CoV in cell cultures in a preliminary study. SARS-CoV was grown in Vero E6 cells cultured in MEM with penicillin G and streptomycin and with 2% fetal bovine serum.

2.3. Human serum samples

Two hundred seventy-six serum samples collected from 156 health care workers in the Hanoi French Hospital, Ho Chi Min city, Vietnam, were used (Vu et al., 2004). Serial serum samples were collected from each of the 120 subjects on different occasions. The sera were used for serological analyses after the heat-inactivation treatment at 56 °C for 30 min.

2.4. Manipulation of infectious SARS-CoV and clinical samples

All procedures that required manipulation of infectious SARS-CoV and/or non-inactivated clinical samples such as neutralizing antibody assay and authentic SARS-CoV antigen preparation were conducted in a BSL-3 laboratories in the National Institute of Infectious Diseases, Tokyo, Japan.

2.5. Recombinant baculovirus

The RNAs were extracted from SARS-CoV (HKU-39849)-infected Vero E6 cells and reverse transcribed using a random hexamer. The N gene of SARS-CoV was then amplified from the random hexamer-primed 1st strand DNAs using a forward primer (N-Bamf: 5′-GGA TCC AAT TAA AAT GTC TGA TAA TGG ACC C-3′, *Bam*HI restriction site is underlined) and a reverse primer (N-Bamr2: 5′-GGA TCC TGC CTG AGT TGA ATC AGC AG-3′, *Bam*HI restriction site is underlined). The PCR product was purified by agarose–gel electrophoresis, cloned into a pGEM-Teasy vector (Promega, Madison, USA) to generate pGEM-Teasy-N, and its sequence was confirmed to be identical to the original sequence (GenBank accession no. AY278491). The N gene insert was excised with *Bam*HI from pGEM-Teasy-N and ligated into the unique *Bam*HI site of a modified pAcYM1 baculovirus-transfer plasmid, pAc-cHis, carrying the 8His-tag at the 3′-extremity of the unique *Bam*HI site. The recombinant baculovirus, *Ac*-SARS-N-His, was then generated using the method described by Kitts et al. (1990).

2.6. Antigens

Vero E6 cells were infected with SARS-CoV for specific antigen production and also mock-infected for control antigen. Extracts of both were made similarly as follows. The authentic SARS-CoV antigen and the corresponding mock-antigen were produced as follows. Vero E6 cell were infected with SARS-CoV or the mock virus at a multiplicity of infection (moi) of 2, respectively. After incubation for 24 h, both the authentic SARS-CoV- and mock-infected Vero E6 cells were collected. The cells were washed twice with cold phosphate-buffered saline (PBS) solution and then suspended in a phosphate-buffered saline solution supplemented with 1% Nonidet-P40 (NP40). Each of the cell-suspended solutions was incubated on ice for 10 min and the cell lysates were centrifuged at 12,000 rpm for 10 min at 4 °C. The supernatant fractions prepared from the SARS-CoV-and mock-infected Vero E6 cells were inactivated by ultraviolet irradiation and were used as positive and negative antigens for IgG ELISA, respectively. The *Tn5* insect cells infected with *Ac*-SARS N-His or with *Ac*-ΔP, a baculovirus not expressing polyhedrin, were incubated for 72 h at 26 °C, respectively. Then both group of cells were washed twice with cold PBS and lysed in cold PBS containing 1% NP40 and 8 M urea. The cell lysates were centrifuged at 12,000 rpm at 4 °C for 10 min. The supernatant fractions were collected as a source of SARS-CoV rNP and negative control antigen for purification. The SARS-CoV rNP and the negative control antigen were purified using a Ni^{2+}-resin purification system (QIAGEN GmbH, Hilden, Germany), according to the manufacturer's instructions.

2.7. IgG ELISA

Authentic SARS-CoV Ag-based and the SARS-CoV rNP-based IgG ELISA were performed as described previously except for the antigen preparation (Saijo et al., 2001, 2002). The antigens were diluted with 50 mM carbonate buffer (pH 9.6) and used to coat the wells of 96-wells ELISA plates in the present study.

2.8. Neutralizing antibody detection

The serum samples were heat-inactivated and diluted two-fold with MEM-2FBS from 1:10 to 1:320. Each test sample (60 μl by volume) was then mixed with the same volume of MEM containing SARS-CoV at an infectious dose of 100 plaque forming units per 100 μl and the mixture was incubated for 1 h at 37 °C for neutralization. After incubation, the mixtures were tested for neutralization by cytopathic effect (CPE) inhibition assay using Vero E6 cells. The neutralizing antibody titer was defined as a reciprocal of the highest dilution at which no CPE was observed.

2.9. SARS-CoV RNA amplification by a loop-mediated isothermal amplification (LAMP) method for detection of SARS-CoV

The SARS-CoV RNA genome was amplified using Loopamp SARS CoV-detection kit (Eiken Chemical, Ohtawara, Japan) as reported previously with some modifications (Hong et al., 2004). RNA was isolated from the serum samples using QIAamp viral RNA mini kit (Qiagen, Germany). Primers used in the Loopamp SARS CoV-detection kit for SARS-CoV RNA amplification were designed according to the nucleotide sequence of Replicase 1b region (GenBank accession number NC_004718). Reverse transcription-LAMP reaction was conducted in 25 μl of the reaction mixture at 62.5 °C for 45 min using the real-time turbidimeter LA200 (TERAMECS, Japan).

2.10. Statistical analysis

Sensitivity, specificity, positive predictive value (PPV) and negative predictive value (NPV) of the SARS-CoV rNP-based IgG ELISA were calculated in comparison with neutralizing antibody assay or with naive SARS-CoV antigen-based IgG ELISA (Qing et al., 2003).

Receiver operating characteristics (ROC) and two-graph-ROC (TG-ROC) curves were analyzed using Stat Flex Version 5 software (Artech Co. Ltd., Osaka, Japan) (Greiner et al., 1995; Qing et al., 2003). The relationship of the OD_{405}s in the SARS-CoV rNP-based IgG ELISA with those of the authentic viral antigen-based IgG ELISA and with the neutralizing antibody titers were evaluated by Spearman's correlation coefficient by rank using Statview software Version 5 (SAS Institute Inc., Cary, NC).

3. Results

3.1. Expression of SARS-CoV rNP

The SARS-CoV rNP was efficiently expressed in the *Tn5* insect cells infected with the recombinant *Ac*-SARS-N-His, and the purified SARS-CoV rNP was visually detected by SDS–PAGE analysis (data not shown).

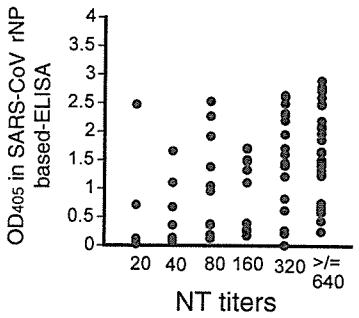

Fig. 1. Plots of the relationship between OD_{405} values at 1:100 by the SARS-CoV rNP-based IgG ELISA and neutralizing antibody titers.

3.2. Relationship of results between the IgG ELISA and neutralizing antibody assay

Of 276 serum samples, 87 showed a positive reaction in the neutralizing antibody assay. The relationship of the neutralizing antibody titers with the OD_{405} values in the SARS-CoV rNP-based IgG ELISA at a dilution level of 1:100 was evaluated using 87 neutralizing antibody-positive samples. There were significant positive correlations between the neutralizing antibody titers and the OD_{405} values in the SARS-CoV rNP-based IgG ELISA (Fig. 1, $R^2 = 0.668$, $p < 0.001$).

3.3. Efficacies of the SARS-CoV rNP-based IgG ELISA in comparison with the neutralizing antibody assay and authentic SARS-CoV-based IgG ELISA

The sensitivity, specificity, PPV and NPV, and ROC area of SARS-CoV rNP-based IgG ELISA were calculated using samples determined to be either positive or negative by neutralizing antibody assay or authentic SARS-CoV-based IgG ELISA. The relative sensitivity and specificity curves of the SARS-CoV rNP-based IgG ELISA using TG-ROC analysis are shown in Fig. 2. The sensitivity, specificity, PPV and NPV of the SARS-CoV rNP-based IgG ELISA were 92%, 92%, 83%, and 96%, respectively, when the cut-off value was set at 0.128 (the OD_{405} value at an intersectional point in Fig. 2b). The ROC area of the SARS-CoV rNP-based IgG ELISA was 0.966 when compared with either the neutralizing antibody assay. The respective values of the SARS-CoV rNP-based IgG ELISA was 94%, 94%, 87%, and 97%, respectively, compared with the naive SARS-CoV antigen-based IgG ELISA, when the cut-off value was set at 0.156 (the OD_{405} value determined in the same way as mentioned above).

3.4. Antibody responses determined by SARS-CoV rNP-based ELISA and neutralizing antibody assay in subjects with sero-conversion

Sero-conversion by neutralizing antibody assay was demonstrated in 19 of the 120 subjects, from whom serial serum samples were collected on different occasions. The sequential changes of OD_{405} in SARS-CoV rNP-based IgG

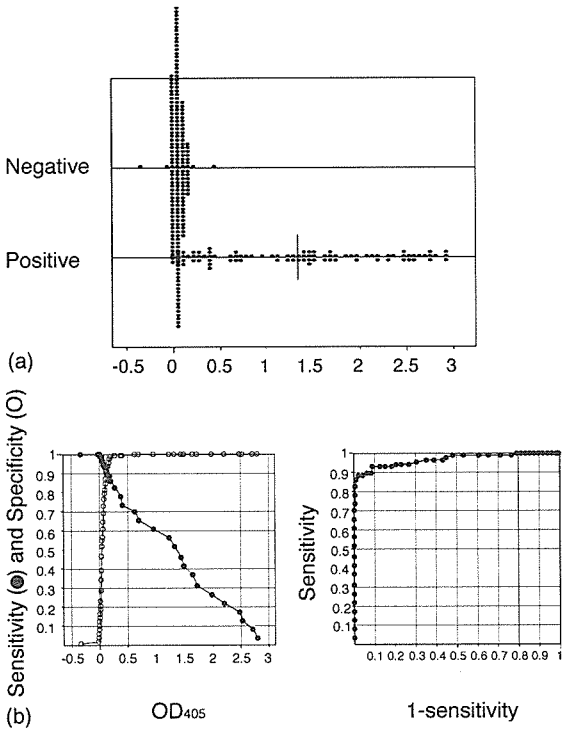

Fig. 2. Plots of (a) the OD_{405} values of the neutralizing antibody-positive and -negative samples measured by the SARS-CoV rNP-based IgG ELISA. The curves of relative sensitivity and specificity of (b) the SARS-CoV rNP-based IgG ELISA by TG-ROC analysis and (c) the ROC curve based on the neutralizing antibody assay.

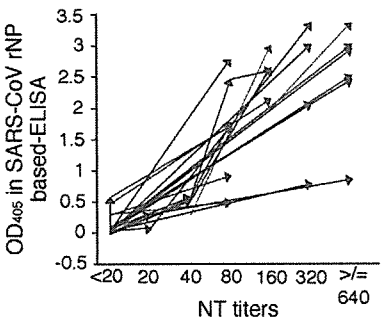

Fig. 3. Sequential change in the OD_{405} value in the SARS-CoV rNP-based IgG ELISA and neutralizing antibody titers in 19 subjects with seroconversion. The terminal positions of the tail and the cap of arrows indicate the level of OD_{405} value in the SARS-CoV rNP-based IgG ELISA at a dilution of 1:100 and neutralizing antibody titers of two serum samples collected from the same subject on different occasions. Black, red and blue arrows indicate the subjects with negative neutralizing antibody and negative antibody detectable by the SARS-CoV rNP-based IgG ELISA at the stage of the first blood collection, those with negative neutralizing antibody but positive antibody detectable by the ELISA at the same stage, and the subjects with positive neutralizing antibody but negative antibody detectable by the ELISA at the same stage, respectively. Green arrows indicate the subjects with both positive neutralizing antibody and positive antibody detectable by the ELISA at the same stage.

ELISA at dilution of 1:100 and neutralizing antibody titers among the 49 serum samples collected from these 19 seroconversion-positive subjects was evaluated (Fig. 3). Each of the serum samples collected first from 17 of the 19 subjects showed a negative neutralizing antibody titer (less than 20)(black, blue or red lines in Fig. 3), while serum samples collected from the other two subjects showed a positive neutralizing antibody titers (green lines in Fig. 3). Four of the 17 neutralizing antibody-negative samples showed a positive reaction in the SARS-CoV rNP-based IgG ELISA (red lines in Fig. 3), while the other 15 showed a negative reaction in neutralizing antibody assay (black or blue lines). Only one sample that showed a positive reaction at a titer of 20 in neutralizing antibody assay showed a negative reaction in the SARS-CoV rNP-based IgG ELISA (blue line in Fig. 3).

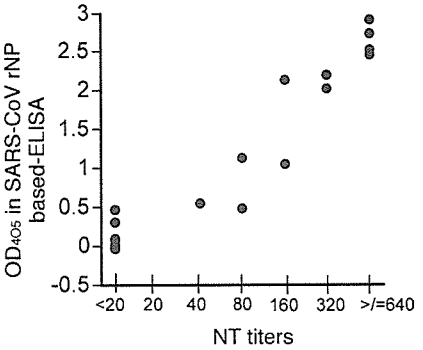

Fig. 4. Plots of the relationship between OD_{405} values at 1:100 by the SARS-CoV rNP-based IgG ELISA and neutralizing antibody titers in the 20 serum samples with positive SARS-CoV genome.

3.5. SARS-CoV RNA amplification and antibodies to SARS-CoV

SARS-CoV RNA was amplified by a LAMP method in 20 serum samples collected from nine subjects. The status of antibody to SARS-CoV in these 20 serum samples was evaluated. Seven of the 20 samples showed a negative reaction in both methods of neutralizing antibody assay and SARS-CoV rNP-based IgG ELISA, two showed a negative reaction in neutralizing antibody assay but a positive reaction in the ELISA, while the other 11 samples showed a positive reaction in both assays (Fig. 4).

4. Discussion

SARS-CoV was revealed to have a 30 kb long viral genome, containing 14 potential open reading frames (ORFs) (8). The sequence of SARS-CoV reveals the presence of ORFs for four structural proteins; i.e., the spike, membrane, envelope and nucleocapsid protein. Among these structural proteins, we selected the nucleocapsid protein, SARS-CoV rNP, as an antigen. Tan et al. recently reported that antibodies to the nucleocapsid and spike proteins of SARS-CoV were demonstrated in 100% of convalescent-phase patients, while antibodies to U274, a protein unique to SASR-CoV, was demonstrated in 73% of the patients (Tan et al., 2004),

indicating that SARS-CoV rNP was the best choice as an antigen among the SARS-CoV structural proteins. Similar results were reported by Woo et al. (2004).

This study was performed using a relatively large panel of serum samples collected from health care workers from a Vietnamese hospital. We developed a recombinant SARS-CoV nucleocapsid protein-based IgG ELISA and confirmed that the ELISA had a higher than 90% sensitivity and specificity in detecting IgG antibodies to SARS-CoV compared with neutralizing antibody assay, the gold standard method, and with the authentic SARS-CoV Ag-based IgG ELISA (Fig. 2). There was a positive correlation between the OD_{405} values in the SARS-CoV rNP-based IgG ELISA and the neutralizing antibody titers (Fig. 1). Furthermore, sequential change in OD_{405} in the SARS-CoV rNP-based IgG ELISA and neutralizing antibody titers in 19 subjects, in whom sero-conversion was demonstrated, was evaluated (Fig. 3). Four of the 19 had already had antibody to SARS-CoV rNP detectable by SARS-CoV rNP-based IgG ELISA, although at this stage they had not yet had a neutralizing antibody equal to or over 20. On the other hand, only one serum sample that showed a positive reaction in neutralizing antibody assay at a titer of 20 showed a negative reaction in the SARS-CoV rNP-based IgG ELISA (Fig. 3). These results suggest that this SARS-CoV rNP-based IgG ELISA is as sensitive as the neutralizing antibody assay. Therefore, it can be concluded that the newly developed SARS-CoV rNP-based IgG ELISA is useful for the serological diagnosis of and seroepidemiological study on SARS-CoV infections.

The SARS-CoV rNP-based IgG ELISA was evaluated for efficacy in detection of specific antibody to SARS-CoV in comparison with neutralizing antibody assay in the present study. There have been several reports on the SARS-CoV rNP-based serological diagnostic system (Chan et al., 2005; Guan et al., 2004; Lin et al., 2003; Shi et al., 2003; Woo et al., 2004). Lin et al. (2003) first reported that SARS-CoV rNP would be one of the candidates for the antigen to detect SARS-CoV antibodies. They confirmed that three of the nine serum samples collected from the patients clinically diagnosed as having SARS showed a positive reaction in SARS-CoV rNP-based Western blotting. The SARS-CoV rNP was then expressed in an *E. coli* system and used as antigen in an antigen-capturing ELISA. It was reported that the antigen-capturing ELISA had high specificity of about 98%, though the sensitivity was not evaluated in the study (Shi et al., 2003). Recently, Guan et al. also reported the efficacy of the recombinant protein of SARS-CoV-based IgG ELISA in diagnosis of SARS (Guan et al., 2004). The SARS-CoV rNP was also expressed in *E. coli* transformed with an expression vector. However, these systems were not compared with the neutralizing antibody assay that is considered to be a gold standard.

The indices of sensitivity, specificity, PPV and NPV of our ELISA were relatively lower than those of the previous reports (Guan et al., 2004; Shi et al., 2003). These differences might be due to differences in the nature of the sera used in the study or due to the methods for the evaluation, or due to the both factors.

The status of antibody to SARS-CoV in the SARS-CoV genome-positive serum samples was evaluated. It was revealed that SARS-CoV genome is still present at a stage of IgG responses in some cases of SARS (Fig. 4). The results indicate that handling of blood collected from patients with SARS must be handled very carefully even if the patients were in a recovery phase with IgG responses. Furthermore, SARS-CoV amplification by a sensitive assay such as LAMP method should be carried out as a diagnostic tool, even when patients with SARS were in a stage of IgG responses.

In summary, a SARS-CoV rNP-based IgG ELISA with high sensitivity and specificity was developed. The advantage of the SARS-CoV rNP-based IgG ELISA is that the antigen can be prepared without the risk of infection.

Acknowledgements

We thank Prof. J.S. Malik Peiris, Department of Microbiology, University of Hong Kong, for providing us with the SARS-CoV (HKU-39849). We also thank Ms. M. Ogata, Department of Virology 1, National Institute of Infectious Diseases, Tokyo, Japan, for her technical assistance. This work is supported by grants-in-aid from the Ministry of Health, Labor and Welfare of Japan.

References

CDC, 2003. Update: outbreak of severe acute respiratory syndrome-worldwide, 2003. MMWR Morb. Mortal Wkly. Rep. 52, 241–248.

Chan, P.K., Liu, E.Y., Leung, D.T., Cheung, J.L., Ma, C.H., Tam, F.C., Hui, M., Tam, J.S., Lim, P.L., 2005. Evaluation of a recombinant nucleocapsid protein-based assay for anti-SARS-CoV IgG detection. J. Med. Virol. 75, 181–184.

Greiner, M., Sohr, D., Gobel, P., 1995. A modified ROC analysis for the selection of cut-off values and the definition of intermediate results of serodiagnostic tests. J. Immunol. Methods 185, 123–132.

Guan, M., Chen, H.Y., Foo, S.Y., Tan, Y.J., Goh, P.Y., Wee, S.H., 2004. Recombinant protein-based enzyme-linked immunosorbent assay and immunochromatographic tests for detection of immunoglobulin G antibodies to severe acute respiratory syndrome (SARS) coronavirus in SARS patients. Clin. Diagn. Lab. Immunol. 11, 287–291.

Hong, T.C., Mai, Q.L., Cuong, D.V., Parida, M., Minekawa, H., Notomi, T., Hasebe, F., Morita, K., 2004. Development and evaluation of a novel loop-mediated isothermal amplification method for rapid detection of severe acute respiratory syndrome coronavirus. J Clin Microbiol 42, 1956–1961.

Kitts, P.A., Ayres, M.D., Possee, R.D., 1990. Linearization of baculovirus DNA enhances the recovery of recombinant virus expression vectors. Nucl. Acids Res. 18, 5667–5672.

Lee, N., Hui, D., Wu, A., Chan, P., Cameron, P., Joynt, G.M., Ahuja, A., Yung, M.Y., Leung, C.B., To, K.F., Lui, S.F., Szeto, C.C., Chung, S., Sung, J.J., 2003. A major outbreak of severe acute respiratory syndrome in Hong Kong. N. Engl. J. Med. 348, 1986–1994.

Lin, Y., Shen, X., Yang, R.F., Li, Y.X., Ji, Y.Y., He, Y.Y., Shi, M.D., Lu, W., Shi, T.L., Wang, J., Wang, H.X., Jiang, H.L., Shen, J.H., Xie, Y.H., Wang, Y., Pei, G., Shen, B.F., Wu, J.R., Sun, B., 2003. Identification of an epitope of SARS-coronavirus nucleocapsid protein. Cell. Res. 13, 141–145.

Poutanen, S.M., Low, D.E., Henry, B., Finkelstein, S., Rose, D., Green, K., Tellier, R., Draker, R., Adachi, D., Ayers, M., Chan, A.K., Skowronski, D.M., Salit, I., Simor, A.E., Slutsky, A.S., Doyle, P.W., Krajden, M., Petric, M., Brunham, R.C., McGeer, A.J., and National Microbiology Laboratory, C.C.S.A.R.S.S.T, 2003. Identification of severe acute respiratory syndrome in Canada. N. Engl. J. Med. 348, 1995–2005.

Qing, T., Saijo, M., Lei, H., Niikura, M., Maeda, A., Ikegami, T., Xinjung, W., Kurane, I., Morikawa, S., 2003. Detection of immunoglobulin G to Crimean-Congo hemorrhagic fever virus in sheep sera by recombinant nucleoprotein-based enzyme-linked immunosorbent and immunofluorescence assays. J. Virol. Methods 108, 111–116.

Saijo, M., Niikura, M., Morikawa, S., Ksiazek, T.G., Meyer, R.F., Peters, C.J., Kurane, I., 2001. Enzyme-linked immunosorbent assays for detection of antibodies to Ebola and Marburg viruses using recombinant nucleoproteins. J. Clin. Microbiol. 39, 1–7.

Saijo, M., Qing, T., Niikura, M., Maeda, A., Ikegami, T., Prehaud, C., Kurane, I., Morikawa, S., 2002. Recombinant nucleoprotein-based enzyme-linked immunosorbent assay for detection of immunoglobulin G antibodies to Crimean-Congo hemorrhagic fever virus. J. Clin. Microbiol. 40, 1587–1591.

Shi, Y., Yi, Y., Li, P., Kuang, T., Li, L., Dong, M., Ma, Q., Cao, C., 2003. Diagnosis of severe acute respiratory syndrome (SARS) by detection of SARS coronavirus nucleocapsid antibodies in an antigen-capturing enzyme-linked immunosorbent assay. J. Clin. Microbiol. 41, 5781–5782.

Tan, Y.J., Goh, P.Y., Fielding, B.C., Shen, S., Chou, C.F., Fu, J.L., Leong, H.N., Leo, Y.S., Ooi, E.E., Ling, A.E., Lim, S.G., Hong, W., 2004. Profiles of antibody responses against severe acute respiratory syndrome coronavirus recombinant proteins and their potential use as diagnostic markers. Clin. Diagn. Lab. Immunol. 11, 362–371.

Tsang, K.W., Ho, P.L., Ooi, G.C., Yee, W.K., Wang, T., Chan-Yeung, M., Lam, W.K., Seto, W.H., Yam, L.Y., Cheung, T.M., Wong, P.C., Lam, B., Ip, M.S., Chan, J., Yuen, K.Y., Lai, K.N., 2003. A cluster of cases of severe acute respiratory syndrome in Hong Kong. N. Engl. J. Med. 348, 1977–1985.

Vu, H.T., Leitmeyer, K.C., Le, D.H., Miller, M.J., Nguyen, Q.H., Uyeki, T.M., Reynolds, M.G., Aagesen, J., Nicholson, K.G., Vu, Q.H., Bach, H.A., Plan, A.J., 2003. Clinical description of a completed outbreak of SARS in Vietnam February–May. Emerg. Infect. Dis. 10, 334–338.

WHO, 2003. Summary of probable SARS cases with onset of illness from 1 November 2002 to 31 July 2003.

Woo, P.C., Lau, S.K., Tsoi, H.W., Chan, K.H., Wong, B.H., Che, X.Y., Tam, V.K., Tam, S.C., Cheng, V.C., Hung, I.F., Wong, S.S., Zheng, B.J., Guan, Y., Yuen, K.Y., 2004. Relative rates of non-pneumonic SARS coronavirus infection and SARS coronavirus pneumonia. Lancet 363, 841–845.

Journal of Medical Virology 75:130–136 (2005)

Protection Against Influenza Virus Infection by Intranasal Administration of Hemagglutinin Vaccine With Chitin Microparticles as an Adjuvant

Hideki Hasegawa,[1]* Takeshi Ichinohe,[1,2] Peter Strong,[3] Izumi Watanabe,[1,2] Satoshi Ito,[1,2] Shin-ichi Tamura,[4] Hidehiro Takahashi,[1] Hirofumi Sawa,[5] Joe Chiba,[2] Takeshi Kurata,[1] and Tetsutaro Sata[1]

[1]*Department of Pathology, National Institute of Infectious Diseases, Musashimurayama-shi, Tokyo, Japan*
[2]*Department of Biological Science and Technology, Tokyo University of Science, Yamazaki, Noda, Chiba, Japan*
[3]*Medical Research Council Immunochemistry Unit, University of Oxford, Oxford, United Kingdom*
[4]*Laboratory of Prevention of Viral Diseases, Research Institute for Microbial Diseases, Osaka University, Yamadaoka, Osaka, Japan*
[5]*Laboratory of Molecular and Cellular Pathology, 21st Century COE Program for Zoonosis Control, Hokkaido University School of Medicine, and CREST, JST, Sapporo, Japan*

Chitin in the form of microparticles (chitin microparticles, CMP) has been demonstrated to be a potent stimulator of macrophages, promoting T-helper-1 (Th1) activation and cytokine response. In order to examine the mucosal adjuvant effect of CMP co-administered with influenza hemagglutinin (HA) vaccine against influenza infection, CMP were intranasally co-administered with influenza HA vaccine prepared from PR8 (H1N1) virus. Inoculation of the vaccine with CMP induced primary and secondary anti-HA IgA responses in the nasal wash and anti-HA IgG responses in the serum, which were significantly higher than those of nasal vaccination without CMP, and provided a complete protection against a homologous influenza virus challenge in the nasal infection influenza model. In addition, CMP-based immunization using A/Yamagata (H1N1) and A/Guizhou (H3N2) induced PR8 HA-reactive IgA in the nasal washes and specific-IgG in the serum. The immunization with A/Yamagata and CMP resulted in complete protection against a PR8 (H1N1) challenge in A/Yamagata (H1N1)-vaccinated mice, while that with A/Guizhou (H3N2) and CMP exhibited a 100-fold reduction of nasal virus titer, demonstrating the cross-protective effect of CMP and influenza vaccine. It is suggested that CMP provide a safe and effective adjuvant for nasal vaccination with inactivated influenza vaccine. ***J. Med. Virol. 75:130–136, 2005.*** © 2005 Wiley-Liss, Inc.

KEY WORDS: influenza; chitin microparticles; nasal vaccine; adjuvant; IgA

INTRODUCTION

Effectiveness and safety are important issues to be considered in the development of a vaccine. The mucosal immune system is usually the first immunological barrier against influenza virus infections [Mestecky and McGhee, 1987]. The respiratory tract mucosa is the primary site of infection and the immunological compartment where the host immune system attacks the influenza virus. Secretory IgA antibodies are major effectors providing a front-line defense against influenza viruses in the respiratory tract mucosa [Shvartsman and Zykov, 1976; Underdown and Schiff, 1986; Murphy, 1994]. The influenza virus causes annual epidemics of influenza, largely due to the selection of new variants with mutations in the surface hemagglutinin (HA). The surface HA determines the antigenic properties of the virus and combines with sialic acid residues on epithelial cells during cell attachment [Renegar and Small, 1994]. Inactivated vaccines against the influenza virus are administered parenterally to induce serum anti-HA IgG antibodies that are highly protective against homologous virus infection, but are less effective against heterologous virus infection [Renegar and Small, 1994; Murphy and Webster, 1996]. In contrast, a large number of studies have shown that the mucosal immunity

*Correspondence to: Hideki Hasegawa, Department of Pathology, National Institute of Infectious Diseases, 4-7-1 Gakuen, Musashimurayama-shi, Tokyo 208-0011, Japan.
E-mail: hasegawa@nih.go.jp

Accepted 9 August 2004
DOI 10.1002/jmv.20247
Published online in Wiley InterScience (www.interscience.wiley.com)

acquired by natural infection, which is largely due to the secreted form of IgA (s-IgA) in the respiratory tract, is more effective and provides greater cross-protection against different virus strains than the systemic immunity induced by parenteral vaccines in human [Clements et al., 1983; Couch and Kasel, 1983; Johnson et al., 1986; Murphy and Clements, 1989; Renegar and Small, 1994] and mice [Liew et al., 1984; Underdown and Schiff, 1986]. In this regard, induction of s-IgA in the RT has a great advantage in protecting against unpredictable epidemics of influenza.

It has been demonstrated that intranasal immunization with an inactivated vaccine together with cholera toxin B (CTB) subunits containing a trace amount of holotoxin (cholera toxin B*, CTB*) induces not only s-IgA with strong cross-protection against infection by virus variants of the same subtype in the upper respiratory tract, but also serum IgG with weak cross-protection against variant virus infection in the lower respiratory tract of mice [Tamura et al., 1988, 1992a,b, 1994b]. These findings were consistent with previous reports [Ramphal et al., 1979; Kris et al., 1985; Nedrud et al., 1987]. Although CTB* is an effective adjuvant for enhancing production of s-IgA, it has some adverse side effects such as producing excessive nasal discharge in humans. Adjuvants which are as effective as CTB* and safe for human use are in great demand for clinical application in nasal vaccination.

Chitin (a natural polysaccharide of *N*-acetyl-D-glucosamine) consisting of microparticles (1–20 μm in diameter) is one of the candidates for an immune enhancing adjuvant, because it can be derived from safe non-microbial sources such as shrimp, crab, and lobster. Chitin is non-allergenic, biodegradable, and biocompatible. Chitin-derived products are now used widely in the medical, veterinary, cosmetic, health supplement, and environmental industries [Okamoto et al., 1993; Strong et al., 2002]. Chitin is also a major component of fungal spores and induces a T-helper-1 (Th1) response. The innate immune system of the lung is well adapted for the clearance of airborne spores largely through phagocytosis by macrophages. This process involves secretion of IL-12 and IL-18 from the macrophages, which enhances Th1 immune responses [Strong et al., 2002]. It has been reported that the intranasal application of chitin microparticles (CMP) results in elevation of Th1 cytokines, including IL-12, IFN-γ, and TNF-α [Schaffner et al., 1982; Strong et al., 2002], and stimulation of a nasal-associated lymphoid tissue by CMP provides a bridge between the innate and adaptive immune systems [Strong et al., 2002]. Chitosan which is the partially deacetylated form of chitin has been used as a vaccine adjuvant due to its muco-adhesive properties, and has been shown to enhance antibody responses to mucosally delivered vaccine antigens [Bacon et al., 2000].

In this study, the mucosal adjuvant activity of CMP was studied when they were intranasally administered with inactivated influenza HA vaccine. It is also demonstrated that nasal CMP-based vaccine resulted in cross-protective immune responses against homologous and heterologous influenza variants.

MATERIALS AND METHODS

Hemagglutinin (HA) Vaccines and Influenza Viruses

HA vaccines (split-product virus vaccines) were prepared from the family Orthomyxoviridae, genus *Influenzavirus A,B*, species *influenzavirus A* including A/Puerto Rico/8/34 (A/PR8; H1N1), A/Yamagata/120/86 (A/Yamagata; H1N1), A/Guizhou/54/89 (A/Guizhou, H3N2) and *influenzavirus B*, B/Ibaraki/2/85 (B/Ibaraki) strains according to the method of Davenport et al. [1964] at the Kitasato Institute (Saitama, Japan). These viruses were grown in the allantoic cavities of 10–11-day fertile chicken eggs, purified and disintegrated with ethyl ether. The vaccine contains all the proteins from the virus particle; however, the major component of the vaccine is HA molecules (about 30% of the total protein). The virus, family Orthomyxoviridae, genus *Influenzavirus A,B*, species *influenzavirus A*, A/Puerto Rico/8/34 (A/PR8; H1N1) used for the challenge experiment was adapted to mice by subculturing 148 times in the ferret, 596 times in the mouse, and 73 times in 10-day fertile chicken eggs.

Adjuvants

CTB subunits containing a trace amount of holotoxin (CTB*) was prepared by adding 0.1% of holotoxin to CTB (Sigma, St. Louis, MO). The CMP were prepared by sonication of dissolved purified chitin (Sigma-Aldrich, Poole, UK) in sterile, endotoxin-free phosphate-buffered saline (PBS). The sonicated chitin particles were collected by centrifugation, washed with 70% (v/v) ethanol, and washed five times with sterile PBS to remove soluble chitin. The diameters of CMP were compared to those of standardized beads, which were 1 and 20 μm in diameter (Polysciences, Inc., Warrington, PA) by flow cytometry (FACS) analysis. The diameters of 98% of the CMP were smaller than 20 μm and 33% were less than 1 μm in size. The sterility of CMP was confirmed by plating onto agar plates, demonstrating no colony formation on the plates. The concentration of endotoxin of CMP solution was examined by a Limulus Amebocyte Lysate Assay (Bio Whittaker, Wokingham, UK) and was shown to be less than 1 EU/ml.

Immunization and Infection With Influenza Virus in Mice

Female BALB/c mice (Japan SLC, Inc., Hamamatsu, Japan), aged 6–8 weeks at the time of immunization, were used in all experiments. All animal experiments were carried out in accordance with the Guides for Animal Experiments performed at NIID and approved by the Animal Care and Use Committee of the National Institute of Infectious Diseases.

Five mice for each experimental group were anesthetized by diethyl ether and immunized primarily by dropping 5 μl of PBS containing either 1 μg of HA vaccines with 10 or 100 μg of CMP, or 1 μg of CTB* into the nostrils. The second immunization was carried out at 4 and 6 weeks later from the primary immunization (three-dose immunization protocol).

According to a modified procedure of Yetter et al. [1980] and Tamura et al. [1996, 1998], each mouse was anesthetized and infected intranasally by dropping 1.2 μl of PBS containing a virus suspension with 1×10^2 PFU of mouse-adapted PR8 virus into each nostril. As 1.2 μl of the virus suspension remained in the local nasal area, the initial viral infection was limited to the nose area.

Measurement of the Virus Titer and Anti-PR8 HA Antibodies of the Samples From the Infected Mice

After complete anesthesia with chloroform, the mice were killed. Serum and nasal wash were collected from the mice for measurement of the virus titer and antibodies against PR8 HA. The levels of IgA and IgG antibodies against HA molecules purified from the A/PR8 viruses were determined by ELISA as described previously [Tamura et al., 1996]. Briefly, ELISA was conducted sequentially from the solid phase (EIA plate; Costar, Cambridge, MA) with a ladder of reagents consisting of the following: first, HA molecules purified from the A/PR8 virus according to the procedure of Phelan et al. [1980]; second, nasal wash or serum; third, goat anti-mouse IgA antibody (α-chain specific anti-IgA antibody; Amersham Biosciences, Piscataway, NJ), or goat anti-mouse IgG antibody (γ-chain-specific anti-IgG antibody; Amersham), or anti-mouse IgG1 and IgG2a (BD Pharmingen, San Diego, CA) conjugated with biotin; fourth, streptavidin conjugated with alkaline phosphatase (Life Technologies, Rockville, MD); and finally, *p*-nitrophenylphosphate. Absorbance was measured at 405 nm using an ELISA reader. A twofold serial dilution of either purified HA-specific IgA or HA-specific monoclonal IgG (160 ng/ml) was used as a standard as described previously [Asahi et al., 2002]. The binding kinetics of the standard HA-specific monoclonal IgG was comparable to purified HA-specific IgG from immunized mice. The IgA and IgG antibody concentrations of unknown specimens were determined from the standard regression curve constructed for each assay with the programmed SJeia Autoreader (model er-8000; Sanko Jun-yaku, Tokyo Japan).

The titers of the subclasses of IgG antibodies against HA molecules were also determined by ELISA. Antibody-positive cut-off values were set at the mean ± 2 SD for pre-immune sera. The antibody titer determined by ELISA was expressed as the highest serum dilution giving a positive reaction. HA-specific monoclonal IgG1 and normal mouse serum were used as controls. The HA-specific monoclonal antibody was recognized exclusively by anti-mouse IgG1 antibody, but not by anti-mouse IgG2a antibody (Fig. 2).

The virus titer was measured as follows: each 200 μl of serial 10-fold dilutions of the nasal wash was inoculated into Madin–Darby canine kidney (MDCK) cells in a six-well plate grown in Dulbecco's modified minimum essential medium supplemented with 10% of fetal calf serum. After 1 hr incubation, each well was overlaid with 2 ml of agar medium according to the method described by Tobita et al. [1975]. The number of plaques in each well was counted at 2 days after inoculation. The experiments were repeated three to five times and the results combined. The data were represented as the mean ± SD.

Statistics

Comparisons between experimental groups were made by Student's *t*-test, and $P < 0.05$ was considered as significant.

RESULTS

Antibody Response to HA and Protection Against Virus Infection in Mice Immunized Intranasally With the HA Vaccine With Chitin Microparticles as an Adjuvant

The mucosal adjuvant efficacy of CMP for influenza HA vaccine was studied. The antibody responses against PR8 HA molecules were examined in mice immunized intranasally with PR8 vaccine together with different amounts (10 or 100 μg) of CMP or 1 μg of CTB* and boosted twice at 4 and 6 weeks after the initial immunization. The secondary anti-PR8 HA IgA antibody responses in the nasal washes and anti-PR8 HA IgG Ab responses in the serum in the immunized mice are shown in Figure 1. The adjuvant effect of CMP was enhanced with an increase of the amount of CMP (Fig. 1). The concentration of s-IgA collected from the nasal wash was more than 100 ng/μl with an average of 140 ng/μl when the mouse was immunized with 10 μg of CMP, and inoculation of 100 μg of CMP with vaccine induced an increase to over 300 ng/μl of the concentration of s-IgA in the nasal mucosa.

Meanwhile, high levels of serum anti-HA IgG responses were induced in mice given 10 μg of CMP with vaccine. The serum IgG responses seemed to parallel the s-IgA response in the nasal wash after immunization with 10 or 100 μg of CMP as adjuvants (Fig. 1). This suggests that intranasal administration of CMP with influenza HA vaccine could induce s-IgA in the nasal area as well as serum IgG.

The IgG subtypes after inoculation of CMP with the HA vaccine were examined (Fig. 2). The IgG2a titer was dramatically increased along with the increase in the amount of CMP (from 10 to 100 μg). This result was consistent with the observation that intranasal application of CMP enhanced Th1 cytokines such as IL-12, INF-γ, and TNF-α [Strong et al., 2002].

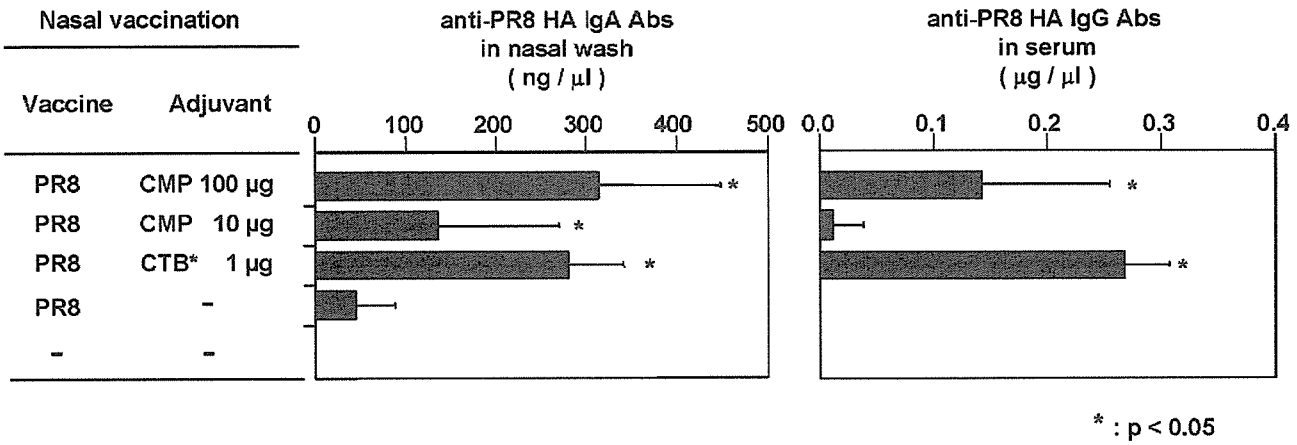

Fig. 1. Anti-PR8 hemagglutinin (HA)-specific IgA in the nasal wash and IgG in the serum from BALB/c mice immunized with intranasal vaccine with 10 or 100 μg of chitin microparticles (CMP), or 1 μg of cholera toxin B* (CTB*) as an adjuvant according to the three-dose regimen. The nasal wash and serum samples were collected at 2 weeks after the third immunization. The antibody titers of five mice from each group were measured by ELISA. The range of anti-HA IgA titers were 187.7–540.0 ng/μl (100 μg of CMP with PR8), 24.9–268.8 ng/μl (10 μg of CMP with PR8), 202.7–347.0 ng/μl (1 μg of CTB* with PR8), and 0–150.8 ng/μl (PR8 alone), respectively. The anti-HA IgA titer was not detected in the non-treated group. The range of anti-HA IgG titers were 0.0–312.1 μg/μl (100 μg of CMP with PR8), 0.0–57.86 μg/μl (10 μg of CMP with PR8), 223.5–327.2 μg/μl (1 μg of CTB* with PR8), respectively. The anti-HA IgG titer was not detected in the group treated with PR8 alone nor in the non-treated group. Each column represents mean ± SD. $*P < 0.05$ versus the value for the group with non-immunized mice (Student's t-test).

Protective Efficacy Against Live Influenza Virus Challenge

The protective effect of intranasal administration of HA vaccine with CMP against influenza viral infection was studied. In control mice, virus titers were $10^{2.9}$ PFU/ml in the nasal wash at 3 days after infection with 1.2 μl of influenza virus (100 PFU) in each nostril (Fig. 3). The mice immunized with HA vaccine without CMP adjuvant showed no protective effect compared with the control mice (Fig. 3). The mice immunized with HA vaccine together with 10 or 100 μg of CMP showed complete protection against the viral challenge infection in a manner similar to the CTB*-treated group (Fig. 3). Thus, intranasal administration of HA vaccine with CMP adjuvant protected the mice against influenza virus infection. This protective effect was consistent with the enhancement of s-IgA and IgG antibody responses after inoculation of HA vaccine with CMP (Fig. 1).

Cross-Protective Effect of Influenza HA Vaccine With Chitin Microparticles as an Adjuvant

To characterize the cross-protective effects of CMP-based intranasal influenza vaccination against variant subtypes of influenza viruses, each group of mice was immunized intranasally with various vaccines (3 μg) together with CMP (100 μg) and boosted 4 and 6 weeks later. At 3 days post infection with A/PR8 (H1N1)

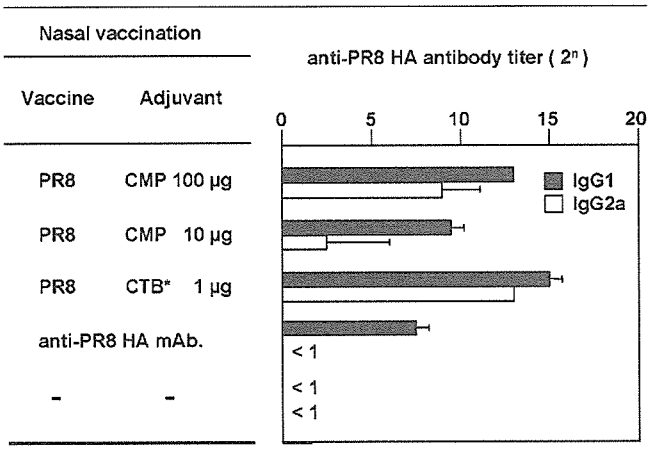

Fig. 2. Anti-PR8 HA-specific subtype of IgGs from BALB/c mice immunized with intranasal vaccine with 10 or 100 μg of CMP, or 1 μg of CTB* as an adjuvant according to the three-dose regimen. The same samples used in Figure 1 were analyzed for IgG subtypes by using IgG1- and IgG2a-specific monoclonal antibodies. HA-specific monoclonal IgG1 and normal mouse serum were used as controls. The antibody titers of five mice from each group were measured by ELISA. Each column represents mean ± SD.

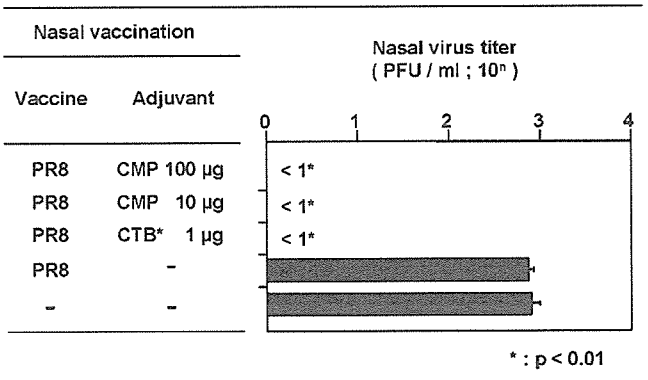

Fig. 3. Virus titers of the nasal washes from mice immunized with intranasal vaccine with 10 or 100 μg of CMP, or 1 μg of CTB* as an adjuvant according to the three-dose regimen. The mice were intranasally infected with 100 PFU of PR-8 influenza virus 2 weeks after the final immunization. The nasal washes were collected at 3 days after the virus challenge. The virus titer was measured by a plaque assay. Each column represents mean ± SD (n = 5). $*P < 0.01$ versus the value for the group with non-immunized mice (Student's t-test).